ROYAL INSTITUTE
OF TECHNOLOGY

Science and Technology for Americium Transmutation

MILAN TESINSKY

Doctoral Thesis
Stockholm, Sweden 2012

TRITA-FYS 2012:21
ISSN 0280-316X
ISRN KTH/FYS/–12:21–SE
ISBN 978–91–7501–326–8

KTH Fysik
AlbaNova Universitetscentrum
106 91 Stockholm

Akademisk avhandling som med tillstånd av Kungliga Tekniska högskolan framlägges till offentlig granskning för avläggande av teknologie doktorsexamen fredagen den 17 augusti 2012 klockan 13:10 i F3.

Tryck: Universitetsservice US AB

Abstract

Americium could be seen as the most troublesome element that is present in nuclear fuel. This thesis offers different points of view on the possibility of americium transmutation. The first point of view elaborates simulations of americium-bearing facilities, namely nuclear data, a popular computational code and modeling techniques. The second point of view is focused on practical usage of the simulations to examine upper limit of americium in a specific reactor.

Sammanfattning

Americium är ett av det mest besvärande elementen i använt kärnbränsle. Denna avhandling behandlar olika aspekter av möjligheten att transmutera americium i snabba reaktorsystem. I den första varianten utarbetas simuleringar och beräkningsmodeller för neutrondatamätningar av betydelse för acceleratordrivna system avsedda att transmutera americium. I den senare undersöks mer praktiska tillämpningar, i synnerhet beräknas gränser för hur mycket americium som kan laddas i bränslet för kritiska bykylda reaktorer.

Acknowledgments


Andrei


Calle

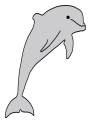
Cecilia


Dear Deer


Janne


Jitka


Luca


Meg

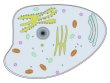
Merja


Mikael


Nils


Odd


Pertti


Pär

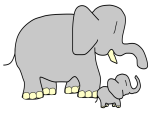
Rodina


Torbjörn


Vasily


Waclaw


Youpeng


Humans

List of Publications

The following papers constitute the thesis:

Included Papers

I **Milan Tesinsky**, Carl Berglöf, Torbjörn Bäck, Boris Martsynkevich, Ivan Serafimovich, Victor Bournos, Anatoly Khilmanovich, Yurii Fokov, Sergey Korneev, Hanna Kiyavitskaya and Waclaw Gudowski, *Comparison of calculated and measured reaction rates obtained through foil activation in the subcritical dual spectrum facility YALINA-Booster*, Annals of Nuclear Energy, 38 (2011), pp. 1412–1417.

`My contribution`: I wrote the paper and made the simulations discussed in the paper. I participated in the post-irradiation gamma measurements of foils in Belarus and carried out the consecutive spectra analysis. I presented the results at the OECD/NEA exchange meeting in Japan, 2009.

II **Milan Tesinsky**, Pernilla Andersson, Cecilia Gustavsson, Stephan Pomp, Michael Österlund, Jan Blomgren, Riccardo Bevilacqua, Anders Hjalmarsson, Anatoly Kolozhvari, François-René LeColley, Nathalie Marie, Alexander V. Prokofiev, Vasily Simutkin and Udomrat Tippawan, *MCNPX Simulations of the SCANDAL Set-up for Measurement of Neutron Scattering Cross Section at 175 MeV*, Physica Scripta, 81 (2010).

`My contribution`: I wrote the paper and performed all the MCNPX simulations. I actively participated in upgrading of the SCANDAL facility and later also in all experimental campaigns using the upgraded setup. I presented the obtained data at the ND2010 nuclear data conference in Korea, 2010.

III **Milan Tesinsky**, Youpeng Zhang and Janne Wallenius, *The impact of Americium on the ULOF and UTOP transients of the European lead-cooled system ELSY*, accepted for publication in Annals of Nuclear Energy.

`My contribution`: I wrote the paper and carried out all the Monte Carlo simulations. I am also the author of the ELSY input file for Serpent.

IV **Milan Tesinsky**, Janne Wallenius, Mikael Jolkkonen and Youpeng Zhang *The impact of Americium on transients in the European lead-cooled system ELSY loaded with nitride fuel*, submitted to Annals of Nuclear Energy.

`My contribution`: I wrote most of the paper and I performed all neutronic calculations and thermohydraulic calculations related to ELSY design modifications.

V **Milan Tesinsky** and Janne Wallenius, *Impact of reflector on Doppler feedback in fast reactors*, to be submitted to Progress in Nuclear Energy.

`My contribution`: I wrote the paper and I am the sole author of all the calculations.

Papers not included in the thesis

Below is a list of papers that are related to the thesis, but not directly included. I am the first author or co-author of all the papers. I have actively participated in the experimental work concerning all of the papers and I was responsible for knowledge dissemination of results presented in some of them.

VI P. Andersson, C. Gustavsson, R. Bevilacqua, J. Blomgren, A. Hjalmarsson, A. Kolozhvari, F.-R. LeColley, N. Marie, M. Österlund, S. Pomp, A. Prokofiev, V. Simutkin, **M. Tesinsky** and U. Tippawan, *An upgrade of the SCANDAL setup for measurements of elastic neutron scattering at 175 MeV*, Radiation Measurements, 45 (2010), pp. 1142–1144.

VII P. Andersson, R. Bevilacqua, J. Blomgren, C. Gustavsson, A. Kolozhvari, F.R. Lecolley, N. Marie, Y. Naitou, L. Nilsson, M. Österlund, S. Pomp, A. Prokofiev, V. Simutkin, **M. Tesinsky**, U. Tippawan and Y. Watanabe, *Measurements of elastic neutron scattering at high energies with SCANDAL at TSL*, EFNUDAT Fast Neutrons - Proceedings of the Scientific Workshop on Neutron Measurements, Theory and Applications - Nuclear Data for Sustainable Nuclear Energy, European Commission, JRC Publication number JRC56548.

VIII R. Bevilacqua, S. Pomp, V. D. Simutkin, U. Tippawan, M. Hayashi, S. Hirayama, Y. Naitou, Y. Watanabe, A. V. Prokofiev, A. Hjalmarsson, P. Andersson, J. Blomgren, M. Österlund, **M. Tesinsky**, F.-R. Lecolley, N. Marie and A. Kolozhvari, *Light-Ion Production in the Interaction of 175 MeV Neutrons with Iron and Bismuth*, Journal of Korean Physical Society, Vol. 59 (2011), Num 2, pp. 1701–1704.

IX R. Bevilacqua, S. Pomp, M. Hayashi, S. Hirayama, Y. Naito, Y. Watanabe, U. Tippawan, V. Simutkin, P. Andersson, J. Blomgren, M. Österlund, **M. Tesinsky**, F.-R. Lecolley, N. Marie, A. Hjalmarsson, A. Prokofiev and A. Kolozhvari, *Study of pre-equilibrium emission of light complex particles from Fe and Bi induced by intermediate energy neutrons*, Journal of Physics: Conference Series, Vol. 312 (2011).

X R. Bevilacqua, S. Pomp, V.D. Simutkin, U. Tippawan, P. Andersson, J. Blomgren, M. Österlund, M. Hayashi, S. Hirayama, Y. Naito, Y. Watanabe, **M. Tesinsky**, F.-R. LeColley, N. Marie, A. Hjalmarsson, A.V. Prokofiev and A. Kolozhvari, *Neutron induced light-ion production from iron and bismuth at 175 MeV*, Radiation Measurements, 45 (2010), pp. 1145–1150.

XI Riccardo Bevilacqua, Stephan Pomp, Vasily Simutkin, Masateru Hayashi, Shusuke Hirayama, Yuuki Naitou, Yukinobu Watanabe, Udomrat Tippawan, **Milan Tesinsky**, Gilles Ban, Jean-Luc Lecouey, François-René Lecolley, Nathalie Marie and Quentin Hamel, *Medley spectrometer for light ions in neutron-induced reactions at 175 MeV*, Nuclear Instruments and Methods in Physics Research Section A: Accelerators, Spectrometers, Detectors and Associated Equipment, Vol. 646 (2011), Issue 1, pp. 100–107.

XII S. Pomp, R. Bevilacqua, M. Hayashi, S. Hirayama, F.-R. Lecolley, N. Marie, Y. Naitou, U. Tippawan, Y. Watanabe, P. Andersson, J. Blomgren, C. Gustavsson, A. Hjalmarsson, A.V. Prokofiev, V.D. Simutkin, E. Tengborn, **M. Tesinsky**, M. Österlund and A. Kolozhvari, *A Medley with over ten years of (mostly) light-ion production measurements at The Svedberg Laboratory*, EPJ Web of Conferences, 8 (2010).

XIII **M. Tesinsky**, P. Andersson, C. Gustavsson, S. Pomp, M. Österlund, J. Blomgren, V. Simutkin, R. Bevilacqua, A. Hjalmarsson, A. Prokofiev, U. Tippawan, F.-R. LeColley, N. Marie, A. Kolozhvari, *Neutron Elastic Scattering Cross-Section Measurements at 175 MeV*, Journal of Korean Physical Society, Vol. 59 (2011), Num 2, pp. 1797–1800.

XIV **Milan Tesinsky**, Carl Berglöf, Andrei Fokau, Boris Martsynkevich, Ivan Serafimovich, Victor Bournos, Anatoly Khilmanovich, Yurii Fokov, Sergey Korneev, Christina Routkovskaia, Hanna Kiyavitskaya and Waclaw Gudowski, *Neutron Flux Characteristics of the YALINA-Booster Core Based on Experiments in Comparison with MCNP Calculations*, Actinide and Fission Product Partitioning and Transmutation – Tenth Information Exchange Meeting, Japan, 2009.

XV U. Tippawan, T. Vilaithong, S. Pomp, P. Andersson, R. Bevilacqua, J. Blomgren, C. Gustavsson, L. Nilsson, M. Österlund, V. Simutkin, H. Sjöstrand, M. Hayashi, S. Hirayama, Y. Naitou, Y. Watanabe, A. Hjalmarsson, A. Prokofiev and **M. Tesinsky**, *Light-Ion Production in 175 MeV Neutron-Induced Reactions on Oxygen*, Journal of Korean Physical Society, Vol. 59 (2011), Num 2, pp. 1979–1982.

XVI Y. Watanabe, Y. Naitou, S. Hirayama, M. Hayashi, A. Prokofiev, A. Hjalmarsson, S. Pomp, P. Andersson, R. Bevilacqua, C. Gustavsson, M. Österlund, V. Simutkin, H. Sjöstrand, **M. Tesinsky** and U. Tippawan, *Characterization of ANITA and QMN Neutron Beams at TSL Using Proton Recoil Techniques*, Journal of Korean Physical Society, Vol. 59 (2011), Num 2, pp. 1439–1442.

XVII Y. Watanabe, S. Hirayama, Y. Naitou, P. Andersson, R. Bevilacqua, C. Gustavsson, M. Österlund, S. Pomp, V. Simutkin, H. Sjöstrand, A. Hjalmarsson, A. Prokofiev, **M. Tesinsky** and U. Tippawan, *Light-Ion Production from a Thin Silicon Target Bombarded by 175 MeV Quasi Monoenergetic Neutrons*, Journal of Korean Physical Society, Vol. 59 (2011), Num 2, pp. 1447–1450.

Contents

Acknowledgments **v**

List of Publications **vii**
Included Papers . . . vii
Papers not included in the thesis . . . viii

Contents **xi**

1 Introduction **1**

2 Nuclear power **5**
2.1 Partitioning and transmutation . . . 7
2.2 Fast reactors . . . 11
2.3 Nuclear fuel for fast reactors . . . 15

3 Minor actinides in fast reactors **23**
3.1 Doppler feedback . . . 23
3.2 Coolant temperature coefficient and coolant void worth . . . 26
3.3 Effective delayed neutron fraction . . . 29

4 Calculation tools **33**
4.1 MCNPX . . . 33
4.2 Serpent . . . 34
4.3 SAS4/SASSYS . . . 34

5 Experimental set-ups **37**
5.1 YALINA-Booster . . . 37
5.2 The SCANDAL set-up . . . 39
5.3 ELSY . . . 42

6 Neutron detection and cross-section measurements **45**
6.1 The tagging technique . . . 46
6.2 The case of hydrogen . . . 47

6.3 The new reaction cross section approach 48
6.4 The improved reaction cross section approach 49

7 Discussion of results and conclusions **51**

A Concluding remarks **53**
A.1 Paper I 53
A.2 Paper II 53
A.3 Paper III 54
A.4 Paper IV 54
A.5 Paper V 55

References **57**

Chapter 1

Introduction

400 000 years ago human learned to control fire [1]. The ability to cook food, to protect us from predators and to produce heat was a turning point in human evolution. For hundreds of thousands of years, renewable sources were successfully used as the fuel for burning. When deforestation made fire wood less accessible, people turned towards the "black stone". Despite the unpleasant fume, coal found its way first to blacksmiths and later also to households of ordinary people.

The major coal boom came in the 18^{th} century. The invention of the steam engine started the *Age of steam* and the coal-fired steam engine became the driving force of the industrial revolution. During the previous century, the internal-combustion engine took the lead, crude oil extraction joined coal mining and burning of fossil fuels reached unprecedented levels. Now, at the beginning of the 21^{st} century human consumes more energy than ever and as much as 85% of the power is produced by burning fossil fuels, namely oil, natural gas and coal. The total world energy consumption by fuel is depicted in Figure 1.1.

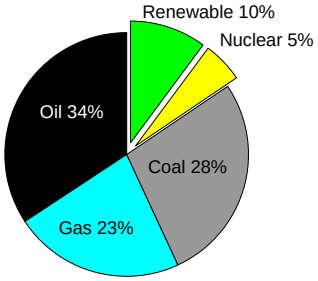

Figure 1.1: *World energy consumption by fuel in 2008 [2]. Notice that the total share of fossil fuels reaches 85%.*

The climate issue

The society as we know it today cannot exist without sources of energy. The fact that fossil fuels represent a limited resource was recognized a long time ago. The official energy statistics from the U.S. government made by the Energy Information Administration (EIA) claim that the coal deposits of the world are still sufficient for more than a century. Namely EIA estimates that the *reserves-to-production ratio*[1] is equal to 126 years [2]. This means that, in principle, the next five generations could rely on coal as a source of energy, because there is enough of it. That is why the scarcity of fossil fuel reserves should not be used as an argument for their replacement; there are other reasons to do so.

At the beginning of this millennium the public turned its attention to another, even more severe problem of fossil fuels. Politicians all around the world started to talk about the relationship between the gradual growth of global temperature (depicted in Figure 1.2) and the long-term increase of carbon dioxide concentration in the atmosphere (shown in Figure 1.3).

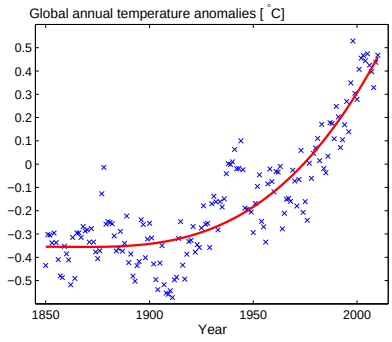

Figure 1.2: *Global annual temperature anomalies since the beginning of continuous temperature records (values relative to the 1961-1990 mean) [3]. Despite the fluctuation, the trend (here in red) is obvious.*

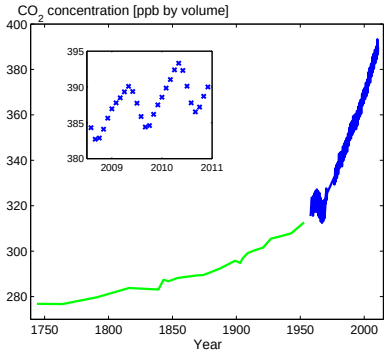

Figure 1.3: *Concentration of atmospheric carbon dioxide in the last 250 years. The green data is obtained indirectly from an analysis of ice core [4] and the blue data originates from direct measurements [5].*

The observed increase in global temperature is a demonstration of more complex changes ongoing in the Earth climate. These changes are together called *global warming*. The majority of climatologists agree that global warming is a consequence of massive fossil-fuel burning; carbon that has been stored underground for millions of years is now rapidly oxidized and released to the atmosphere. The real conse-

[1] The Reserves-to-production ratio is the remaining amount of a non-renewable resource, expressed in years.

quences of global warming are unknown, but predictions expect large-scale negative impact on most of the population [6].

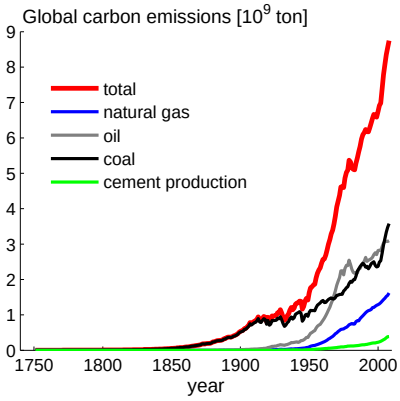

Figure 1.4: *Global carbon emissions by source [7]. Vast majority or the emissions is emitted by incineration for energy production, i.e. burning of oil, coal and natural gas.*

Carbon dioxide accounts for the second largest contribution to the global warming, after water vapor [8]. Most of the CO_2 emissions are connected with energy production, as shown in Figure 1.4.

Table 1.1: Life-cycle emissions of CO_2, CH_4 and N_2O according to energy source as published by IAEA [9]. For comparison there is also the production of CO_2 from electricity generation in the Nordic countries as estimated by Vattenfall [10]. CO_2eq [g/kWh] stands for gram of equivalent CO_2 per kilowatt-hour of electricity.

Energy source	**IAEA** CO_2eq [g/kWh]	**Vattenfall** CO_2 [g/kWh]
Nuclear power	3–24	3
Hydro power	1–34	5
Wind power	8–30	10
Bio-fueled CHP[2]	-	10
Solar power	44–76	60
Natural gas	400–800	400
Coal	760–1280	700
Back-up gas turbines	-	1300

Availability and efficiency of energy resources varies in different parts of the world and so does the production of CO_2 even from the same source. Because of

[2]CHP stands for Combined Heat and Power

this variation, it is impossible to relate one energy source to an exact and universal production of carbon dioxide. The International Atomic Energy Agency (IAEA) made a comparative study of different energy sources according to their contributions to the global warming [9]. In this life-cycle analysis IAEA takes into account not only CO_2, but also other gases that contribute to global warming. Some results of the study are presented in Table 1.1 together with data published by the Swedish energy utility Vattenfall. In its report, Vattenfall estimates the emissions of fossil carbon dioxide from generation of electricity delivered to household customers in Sweden [10]. Even though there is a rather large spread in the data from IAEA, it is clear that nuclear power is one of the most climate-friendly source of energy.

Many countries all over the world are attracted by the idea of a power station that produces hundreds of megawatts for more than 300 days a year, does not need much of imported fuel and moreover is climate-friendly. According to the IAEA, in May 2012 there were 30 countries having 436 nuclear power reactors in operation with a total net installed capacity of 370.499 GW_e. Additional 62 nuclear power reactors are under construction [11].

Nuclear power has, however, also some disadvantages. Some of them are discussed in **Chapter 2**. The impact of minor actinides (produced by nuclear power operation) on fast reactors is elaborated in **Chapter 3**. The following **Chapters 4, 5 and 6** describe calculation and experimental methods and tools leading to the conclusions presented in **Chapter 7**. The last **Chapter A** gives more details bout the papers included in the thesis.

Chapter 2

Nuclear power

In a nuclear power reactor energy is gained from fission of heavy nuclei into fission products. Traditionally, the heavy nucleus to be fissioned is uranium and the fission products could include virtually any element lighter than uranium. Most of the nuclear power reactors are using simple uranium dioxide, UO_2, as a fresh input fuel and produce significantly more complicated irradiated fuel during their operation. An example of typical irradiated fuel composition is given in Table 2.1. Except for ^{235}U and ^{238}U all isotopes are created during the irradiation and were not present in the fresh fuel.

It is interesting that a number of isotopes in the irradiated fuel are neither uranium from fresh fuel nor fission products. Namely all isotopes of plutonium, americium and curium are heavier than the original atoms of the fresh fuel and therefore could not be created by fission of uranium. These so called *transuranium elements* (TRU) are produced by neutron capture, i.e. an event when the neutron is absorbed by an atom and stays there to create a heavier isotope. Plutonium forms the majority of the trans uranium elements; the other elements are called *minor actinides* (MA).

Building of heavier isotopes through neutron capture in combination with decay into lighter isotopes create typical paths on the table of nuclides, so called *transmutation chains*. There are three major transmutation chains:

The uranium-plutonium chain

$$^{238}U \xrightarrow{capture} {}^{239}U \xrightarrow{\beta^- decay} {}^{239}Np \xrightarrow{\beta^- decay} {}^{239}Pu$$

The minor actinide chain

$$^{241}Pu \xrightarrow{capture} {}^{242}Pu \xrightarrow{capture} {}^{243}Pu \xrightarrow{\beta^- decay} {}^{243}Am \xrightarrow{capture} ...$$
$$...{}^{244}Am \xrightarrow{\beta^- decay} {}^{244}Cm \xrightarrow{capture} {}^{245}Cm \xrightarrow{capture} {}^{246}Cm$$

Table 2.1: Isotopic composition of irradiated UOX fuel with 4.2% initial enrichment after 50.05 GWd/tHM burning and four years of cooling [12]. In the table c is the isotopic fraction, $T_{1/2}$ is the half-life and ϵ is the effective dose coefficient for ingestion [13].

Isotope	c [%]	$T_{1/2}$ [a]	ϵ [mSv/kBq]
^{235}U	6.5	703,800,000	47
^{236}U	4.8	23,420,000	47
^{238}U	78.6	1,468,000,000	45
^{237}Np	0.06	2,144,000	110
^{238}Pu	0.04	87.7	230
^{239}Pu	0.53	24,110	250
^{240}Pu	0.24	6,564	250
^{241}Pu	0.13	14	4.8
^{242}Pu	0.08	373,300	240
^{241}Am	0.03	432	200
^{242m}Am	10^{-4}	141	290
^{243}Am	0.02	7,370	200
^{243}Cm	10^{-4}	29	150
^{244}Cm	0.01	18	120
^{245}Cm	10^{-3}	8,500	210
^{246}Cm	10^{-4}	4,760	210
^{79}Se	10^{-3}	650,000	2.9
^{90}Sr	0.14	29	28
^{93}Zr	0.23	1,530,000	1.4
^{99}Tc	0.25	211,100	0.6
^{107}Pd	0.06	6,500,000	0.04
^{126}Sn	10^{-3}	100,000	4.7
^{129}I	0.04	15,700,000	110
^{135}Cs	0.09	2,300,000	2
^{137}Cs	0.27	30	13
Other fission products	7.9	NaN	NaN

The cyclic chain

$$\uparrow \quad \xrightarrow{capture} {}^{240}Pu \xrightarrow{capture} {}^{241}Pu \xrightarrow{\beta^- decay} {}^{241}Am \xrightarrow{capture} \quad \downarrow$$
$${}^{239}Pu \xleftarrow{capture} {}^{238}Pu \xleftarrow{\alpha decay} {}^{242}Cm \xleftarrow{\beta^- decay} {}^{242}Am$$

The transuranium elements as well as the fission products are harmful to the environment and have to be separated from the biosphere. The harmful effect of chemical substances as a result of their content of radioactive elements is called *radiotoxicity*. The radiotoxicity depends on the type and intensity of the radiation emitted by the element.

Luckily, all radioactive elements decay and their concentration decreases in time and so does the radiotoxicity. Figure 2.1 shows gradual decrease of the radiotoxicity of a typical spent fuel. A careful reader can notice that in spite of the relatively longer half-life of some fission products, the long-term radiotoxicity is dominated by transuranium elements. In particular, after 500 years it is virtually only plutonium and americium that cause the radiotoxicity of irradiated fuel to exceed its original value. The next chapter presents and develops the idea of separating americium and plutonium from the irradiated fuel.

2.1 Partitioning and transmutation

As described in the previous chapter, it appears beneficial to separate fission products and transuranic elements from the irradiated nuclear fuel; this is so called *partitioning*. The fission products could be loaded into a final repository and would decay during a relatively short time. The transuranic elements could possibly be either used as new fuel or *transmuted*, i.e. converted into other isotopes with a shorter half-life. For burning of plutonium and transmutation of minor actinides one of the following three reactor concepts could be used.

Light-water reactor

There are two types of traditional light-water reactors (LWR): the pressurized water reactor (PWR) and the boiling water reactor (BWR). In both cases, light water is used as a moderator and coolant at the same time. The LWR technology is proven and widely spread across different countries, so it is a natural candidate for plutonium burning and minor actinide transmutation.

Plutonium recycling is done today in a so called mix-oxide fuel (MOX). In MOX fuel part of the fissile uranium ^{235}U is replaced by plutonium extracted from a previously irradiated fuel; usually about 10% of uranium is substituted by plutonium. MOX fuel not only burns plutonium, but it also reduces needs for the expensive process of uranium enrichment.

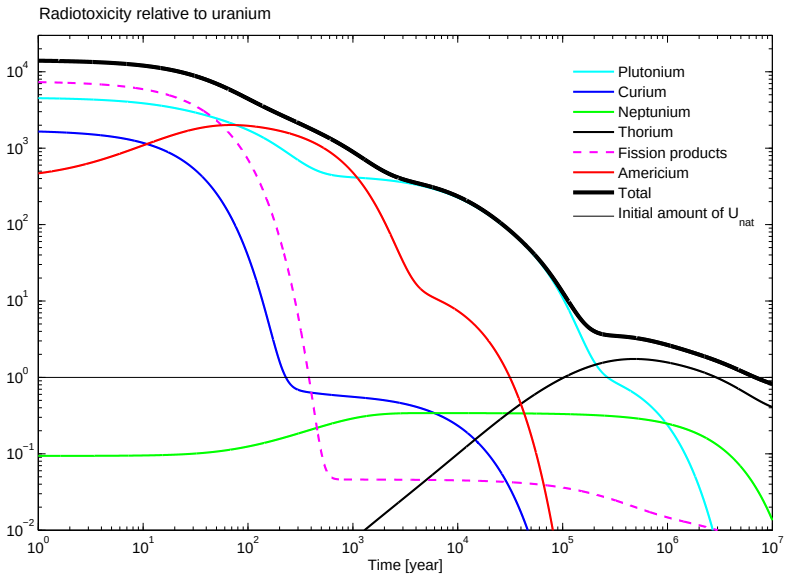

Figure 2.1: *Decay of the radiotoxicity of typical irradiated fuel (for details about the fuel see Table 2.1) compared to the radiotoxicity of the initial amount of pure natural uranium needed for production of the original fresh fuel. Note that it takes about ten million years for the induced radiotoxicity to decay back to the initial level.*

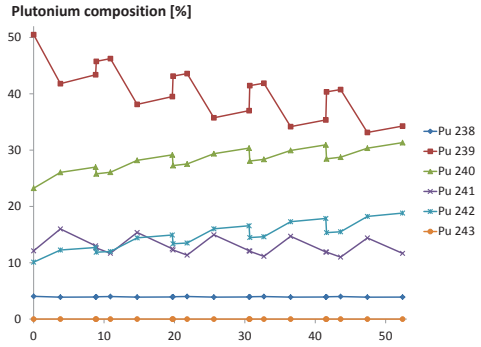

Figure 2.2: *Weight fractions of plutonium isotopes during multi-recycling of MOX fuel in PWR. Each cycle starts with irradiation (3.8 years) followed by cooling (5 years), reprocessing (instant) and additional cooling (2 years) before new irradiation. The figure shows five irradiations. (MOX with 9% PuO_2, 3% U enrichment, burnup 48 GWd/tHM)*

Unfortunately, simple homogeneous multi-recycling of plutonium in LWR deteriorates safety parameters. Figure 2.2 shows degradation of plutonium isotopic vector during five consecutive recycling periods in PWR. The fissile isotopes ^{239}Pu and ^{241}Pu are gradually replaced by fertile isotopes ^{240}Pu and ^{242}Pu. The *fission probability*[3] of ^{240}Pu depicted in Figure 2.3 increases rapidly at neutron energies above 10 keV. This increase is a potential safety problem; if the moderator is partly removed, the neutron energy increases and more fission is induced. For example a potential water boiling in PWR would therefore lead to a positive reactivity feedback. The coolant void worth of PWR with plutonium composition shown in Figure 2.2 changes from -4650 pcm at the beginning of the first cycle to +4130 pcm at the end of the fifth cycle; a strongly negative reactivity feedback is changed to a strongly positive feedback and that is not acceptable.

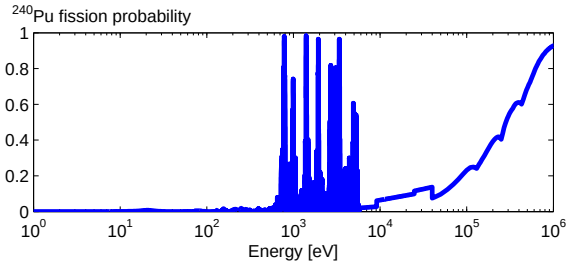

Figure 2.3: *Fission probability of ^{240}Pu has a threshold and grows significantly for neutron energies above the threshold. Similar behavior is observed also for ^{238}Pu and ^{242}Pu.*

This issue could be tackled by adding additional fissile isotopes to multi-recycled MOX fuel. The fission probability of fissile isotopes decreases in harder spectrum and this reduction could compensate the positive feedback of fertile isotopes. An easily obtained fissile isotope is ^{235}U, which could be added to MOX fuel in homogeneous mixing (so called MOX-UE), or in a heterogeneous manner (so called CORAIL assembly) as first described by Youinou and Vasile [14].

The presence of americium in LWR fuel makes the problem with void worth even worse. As indicated in the cyclic transmutation chain, ^{241}Am is transmuted into ^{242}Am which decays first into ^{242}Cm and then into ^{238}Pu. As explained in the previous paragraph, introduction of ^{238}Pu could result in changing the originally negative reactivity feedback to positive.

[3]Fission probability is the probability that a neutron that is absorbed by the nucleus induces fission. For neutron absorption the other complementary process to fission is capture.

Dedicated burner

As it was shown in the previous chapter, americium burning in LWR compromises reactivity feedbacks and consequently also the safety of LWR. It has been therefore suggested to consider a design of a reactor core that would be purely dedicated to minor actinides and possibly also plutonium burning. A subcritical source-driven core that is less sensitive to reactivity feedbacks could be such a dedicated burner. This idea first appeared in open literature about forty years ago [15] and was reborn twenty years later [16].

The accelerator-driven system (ADS) as depicted in Figure 2.4 is a coupling of a subcritical core to a neutron source. The neutron source is often designed in the form of a spallation target bombarded by protons accelerated in a cyclotron[4] to very high energies. Neutron yield from a tungsten spallation target published by Bauer shows in Figure 2.5 that the energy of spallation neutrons can reach nearly the same value as the originally accelerated proton [17].

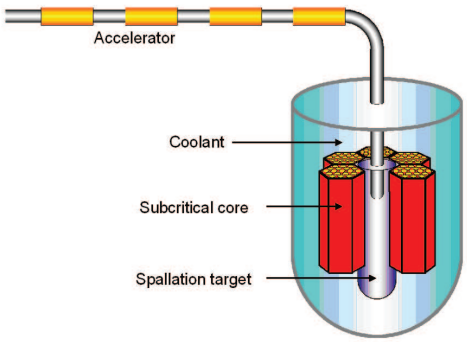

Figure 2.4: *Schematic picture of an accelerator-driven system (ADS).*

The relatively lower sensitivity of ADS to increased content of minor actinides and to lower plutonium quality makes it possible to load and burn long lived transuranium elements effectively and on a large scale [18]. ADS can therefore be introduced in the nuclear fuel cycle even after many decades of LWR operation, when large quantities of TRU have accumulated [19]. Unfortunately, technical issues connected with the spallation target do not allow construction of ADS today. Last but not least also the cost of energy produced in ADS is relatively higher and could not compete with the cost of electricity produced in standard LWR. If ADS is ever going to be deployed for irradiated fuel radiotoxicity reduction, the society must be ready to pay the price.

[4]Cyclotron is an accelerator that accelerates particles using a combination of magnetic and electric fields. The accelerated particle follows a nearly circular trajectory reaching higher and higher speed with every circle.

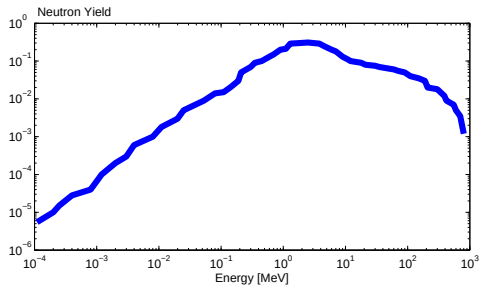

Figure 2.5: *Neutron yield of a tungsten spallation target bombarded by 800 MeV protons [17].*

Fast Reactors

It has been shown that even fast-spectrum critical systems could at least match the burning capability of ADS [20]. Unlike ADS, fast reactors (FR) have been built and successfully operated. Also electricity produced in fast reactors is cheaper compared to ADS. The next chapter elaborates fast reactors more in details.

2.2 Fast reactors

At the beginning of this millennium ten leading countries took the initiative, discussed the future of nuclear power and signed the Generation IV International Forum (Gen IV Forum) Charter [21]. Argentina, Brazil, Canada, France, Japan, the Republic of Korea, the Republic of South Africa, the United Kingdom and the United States were shortly followed by Switzerland, Euratom, the People's Republic of China and the Russian Federation. In the charter the member countries specify eight goals for future Gen IV energy systems. These goals are

- **Sustainability-1** Requirement for *"effective fuel utilization"*.
- **Sustainability-2** Reduction of the amount of long-term radiotoxic irradiated fuel.
- **Economics-1** Cost competitiveness with other energy sources.
- **Economics-2** Financial risk comparable to other energy sources.
- **Safety and Reliability-1** Excellent safety and reliability.
- **Safety and Reliability-2** Very low likelihood and degree of reactor core damage.
- **Safety and Reliability-3** No need for offsite emergency response.

- **Proliferation Resistance and Physical Protection** Make Gen IV systems *"very unattractive"* for weapon production.

Six reactor concepts that could possibly reach the goals were identified in the Gen IV roadmap [22]. The six reactor concepts are

- **Gas-Cooled Fast Reactor System (GRF)**
- **Lead-Cooled Fast Reactor System (LFR)**
- Molten Salt Reactor System (MSR)
- **Sodium-Cooled Fast Reactor System (SFR)**
- Supercritical-Water-Cooled Reactor System (SCWR)
- Very-High-Temperature Reactor System (VHTR)

The goal for *"effective fuel utilization"* in combination with U-Pu cycle can only be reached in a fast neutron spectrum, so it is not a surprise that three out of the six concepts are fast reactors (in bold). In the next three chapters these systems are elaborated more in details.

Sodium-Cooled Fast Reactor

Sodium exhibits a number of excellent physical properties suitable for a fast-reactor coolant: extremely low neutron capture cross section, very high thermal conductivity, high thermal capacity and relatively low density. The melting temperature is unfortunately above the standard room temperature, but still easily achievable. Table 2.2 summarizes basic properties of sodium and lead.

Table 2.2: Selected physical properties of sodium and lead. k is thermal conductivity, C_p is thermal capacity, ρ is density, T_{boil} is the boiling temperature and T_{melt} is the melting temperature.

Coolant	$k\ \left[\frac{W}{mK}\right]$	$C_p\ \left[\frac{J}{kg \cdot K}\right]$	$\rho\ \left[\frac{kg}{m^3}\right]$	T_{boil} [°C]	T_{melt} [°C]
Sodium	68	1277	850	883	98
Lead	17	147	10,500	1,743	328

Hot sodium cannot be used directly to spin a turbine and a steam generator for water-vapor production is still required, as shown in the schematic diagram of SFR in Figure 2.6. Sodium, however, reacts violently with water in an exothermic reaction producing hydrogen

$$2Na + 2H_2O \rightarrow 2NaOH + H_2. \tag{2.1}$$

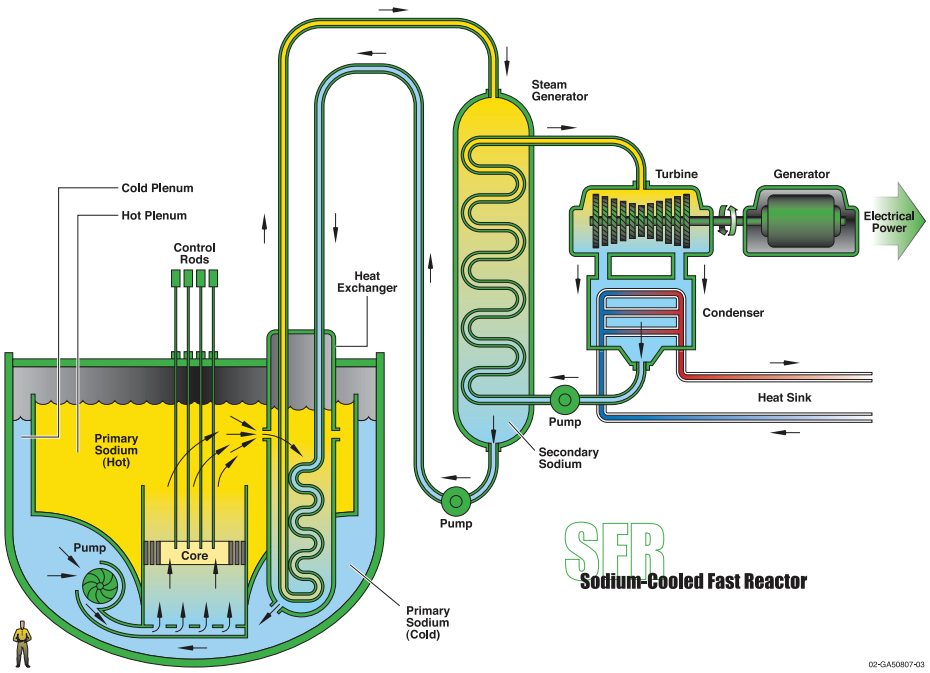

Figure 2.6: *Schematic layout of the sodium-cooled fast reactor [22].*

It is thus necessary to avoid a direct contact between sodium and water. Construction of the steam generator becomes therefore technically difficult and expensive. Other extra costs are associated with intermediate sodium loop which connects the radioactive sodium inside the core with the non-active water in the turbine.

The very high thermal conductivity of sodium makes it possible to decrease the pitch between fuel pins. Tight lattice of SFR minimizes neutron leakage from the core and sodium-cooled fast reactors exhibit an excellent neutron economy and high breeding ratio[5]. Technical feasibility of the SFR concept has been proved in a number of countries.

With the low boiling point below 900°C, it is necessary to consider scenarios with partial or complete removal of liquid sodium from the core. In such a case fewer neutrons are absorbed in the coolant leading to a positive reactivity feedback. The positive void worth is a serious safety problem of all SFRs and has to be addressed in each individual design.

[5]Breeding ratio is the ratio between produced and consumed fissile isotopes. High breeding ratio is required for *"effective fuel utilization"*.

Lead-Cooled Fast Reactor

For the first sight, lead has significantly worse physical characteristics compared to sodium. The neutron capture cross section is more than three times higher, the thermal conductivity is more than three times lower and the thermal capacity is almost ten times lower. Also the melting temperature is somewhat high, so it becomes more demanding to prevent solidification of lead.

On the other hand, lead has some other attractive properties. The boiling temperature of lead is very high which makes coolant boiling virtually impossible. There is no rapid chemical reaction between lead and water making the reactor cheaper to build; steam generators could be located directly in the vessel and (as seen in Figure 2.7) there is no need for intermediate loop.

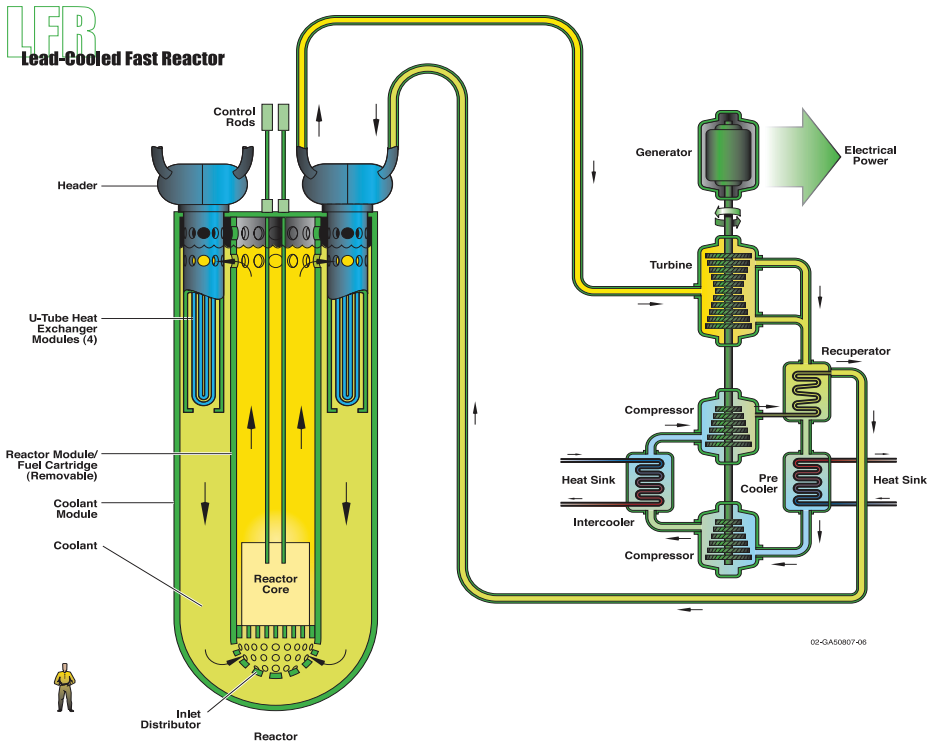

Figure 2.7: *Schematic layout of the lead-cooled fast reactor [22].*

Lead features also other safety-related advantages compared to SFR and LWR. Lead by itself has superior shielding properties and physically blocks harmful radiation coming from the fission process and irradiated fuel. Besides that, lead also forms chemical compounds with iodine and cesium and retains thus the most

problematic fission products in case of cladding failure. The high density of Pb is to some extend compensated by a high degree of natural circulation. Natural circulation plays a vital role for decay heat removal during accident scenarios.

So far, the lead-cooled technology has been used only in military applications mainly for two reasons: it is energetically demanding to prevent lead from freezing and lead has strongly erosive and corrosive properties leading to severe physical and chemical deterioration of any known material suitable for fuel cladding and especially pump blades. Ongoing research activities try to address the material issues, but at the moment, there is no complete solution for a power reactor. As shown by Wallenius et al., for a limited core power of a training reactor, it is possible to rely on natural circulation of lead and avoid pumps completely [23].

Gas-Cooled Fast Reactor

The gas-cooled reactor concept is very different from SFR and LFR, because the coolant is gaseous and not liquid. On one hand, gaseous coolant brings some advantages, such as no need for steam generator - hot gas is used in a direct turbine cycle to spin a turbine as depicted in Figure 2.8. Also chemical interaction with water, cladding, pumps and any other materials virtually does not exist.

On the other hand, gaseous coolant has to be used under high pressure to ensure sufficient heat removal capabilities. In accident scenarios with loss of pressure it is challenging to design passive cooling systems and an active system is required for decay heat removal. Because any active system has non-zero possibility to fail, it becomes difficult to ensure *"excellent safety and reliability"*, which is one of the goals for Gen IV systems. The safety issues related to loss of pressure are certainly one of the reasons why so far, there is no operational experience of GFR.

2.3 Nuclear fuel for fast reactors

The fuel itself is a key component of any nuclear power plant. It is the fuel that produces heat and all other components of the reactor are present just to utilize and control the heat production in a safe manner. Operation of a fast reactor sets specific demands on the fuel material. Kittel et al. list the following seven requirements [24]:

- High fissile atom density
- High thermal conductivity
- Good compatibility with the fuel cladding and reactor coolant
- As few moderating atoms as possible
- A uranium analogue for the blanket
- High gas release and low swelling from solid-state fission products

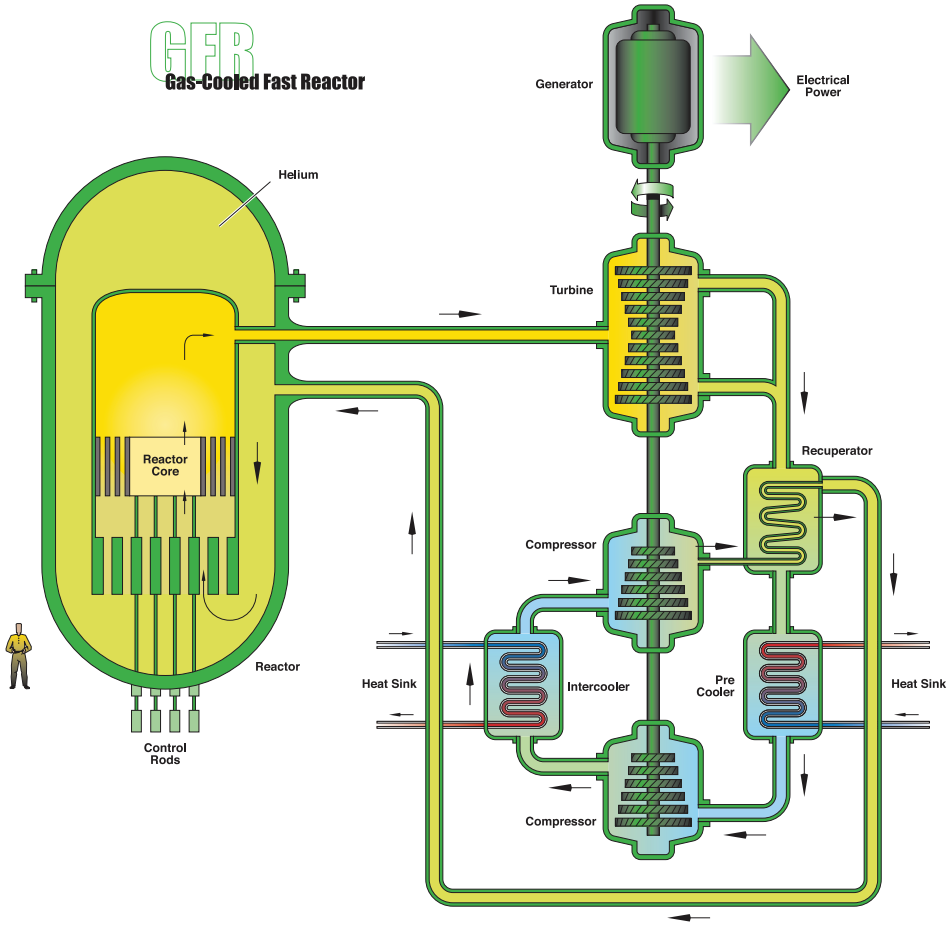

Figure 2.8: *Schematic layout of the gas-cooled fast reactor [22].*

- A high melting point

In the past scientists have tried to address simultaneously as many requirements as possible and the following four fuel types have been so far used for fast reactor operation [24]:

- **Oxide fuels** operated in many reactors including Super-Phenix in France and BN600 in Russia.
- **Metallic alloy fuels** utilized in the dawn of nuclear power e.g. in Clementine and EBR reactors in USA.
- **Carbide fuels** in recently shut-down BR-10 in Russia and in Indian FBTR.
- **Nitride fuels** used in BR-10.

The following four chapters describe advantages and disadvantages of the above mentioned fuel types. A list of basic pros and cons is summarized at the end in Table 2.4.

Oxide fuels

Oxide fuels are widely used in the most common type of reactors today, namely in LWR. The relatively easy fabricability, in combination with excellent thermal stability, makes the oxide fuel an interesting candidate also for fast reactors. On the other hand, low thermal conductivity and high stoichiometry of light atoms (oxygen) are major drawbacks of oxide fuels.

Oxide fuels for FR consist of MA oxides, mainly uranium, plutonium and americium oxides. The uranium oxide is stable simply as a uranium dioxide, UO_2, but the case is more complicated for plutonium and americium. Plutonium oxide is not exactly a dioxide, but exists in a sub-stoichiometric state denoted as PuO_{2-x}. The value of x is not constant and depends on temperature and chemical environment. For example pure MOX fuel is typically produced with oxide-to-metal ratio between 1.95 and 1.98. When americium is added to MOX, the oxide-to-metal ratio decreases to about 1.90 [25].

Oxide fuels feature excellent thermal stability in comparison with the other fuel candidates. A fuel failure could occur with temperature values above the solidus or liquidus temperatures[6]. The solidus temperature could be calculated using the modified Vegad's law

$$T_{solidus} = \sum_{i \in \{UO_2, PuO_2, AmO_2\}}^{n} T_i^{melting} \cdot c_i + C_{burnup} + C_{stoichiometry}, \qquad (2.2)$$

[6]The solidus temperature denotes the point at which a material becomes completely solid. The liquidus temperature, on the other hand, denotes the point at which a material becomes completely liquid.

where $T_i^{melting}$ and c_i are melting temperatures and atomic fractions of UO_2, PuO_2 and AmO_2. As indicated by constants C_{burnup} and $C_{stoichiometry}$, the solidus temperature decreases with burnup and deviation from the strict 2+1 stoichiometry. The melting temperatures $T_i^{melting}$ vary significantly in different sources. Recent measurements listed in Table 2.3 provide the most reliable results [26, 27].

Table 2.3: Recently published melting temperatures of MA oxides.

Oxide	$T^{melting}$ [°C]
UO_2	2857 ± 30
PuO_2	2744 ± 28
AmO_2	2500 ± 16

High thermal conductivity of nuclear fuel is a clear benefit; heat produced in the fuel has to be transported to the coolant and the higher is the thermal conductivity of the fuel, the easier is the process. low thermal conductivity, on the other hand, results in a high temperature gradient between the inner and outer parts of the fuel.

Thermal conductivity, λ, of unirradiated (U,Pu)O_{2-x} MOX fuel with 100% theoretical density can be described as [28, 29, 30]

$$\lambda(T,x) = \frac{1158}{A(x)+B(x)T} + C\left(\frac{1000}{T}\right)^{\frac{5}{2}} exp\left(-\frac{D}{T}\right), \tag{2.3}$$

where x is the deviation from the 2+1 stoichiometry and

$$A(x) = 0.035 + 2.85x \tag{2.4}$$

$$B(x) = 0.286 - 0.715x \tag{2.5}$$

$$C = 6400 \tag{2.6}$$

$$D = 16,350. \tag{2.7}$$

Thermal conductivity of MOX fuel calculated according to Eq, 2.3 is depicted in Figure 2.9. From this comparison, it is clear that in this aspect, oxide fuel is loosing against the other options.

Metallic alloy fuels

Metallic alloy fuels have the ultimate concentration of actinides and exclude completely light atoms leading to a very hard neutron spectrum. Thermal conductivity is unbeatable and high thermal expansion can to some extend even substitute the

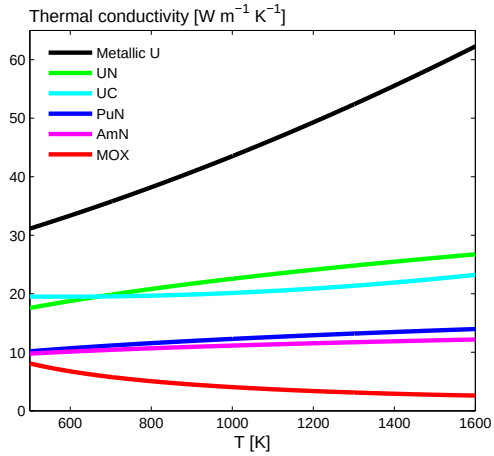

Figure 2.9: *Thermal conductivity of different fuels.*

negative Doppler reactivity feedback. On the other hand, metallic alloy fuels suffer significant swelling under irradiation and the high thermal expansion brings along large gap between fuel and cladding.

Separation of metallic uranium and plutonium from other compounds, such as fission products, is easily done by electrolytic separation in metallic melt [31, 32]. Fuel pins are later formed by pouring the melt in a crucible, so the whole fabrication process is completely dust-free. Unfortunately, the same procedure cannot be applied to americium bearing fuel, because liquid americium is volatile and much of it is lost during the fabrication process.

Metallic alloy fuels have a very low solubility of helium and gaseous fission products leading to a very large swelling. In order to avoid fuel-clad mechanical interaction, metallic alloy fuels should be fabricated with low smear density, usually 75%. The gap between fuel and clad thus occupies as much as one quarter of the volume and becomes a major obstacle for heat transfer between the fuel and coolant. Helium usually used as an inert gas in the gap has too low thermal conductivity and has to be replaced by sodium. Sodium, however, penetrates the fuel during burnup. At the end of fuel cycle, metallic alloy fuels using the sodium bond are not suitable for reprocessing using the standard PUREX[7] method.

Metals have in general good thermal conductivity and actinides are not an exception. Thermal conductivity of metallic uranium increases with the second power of temperature as [33]

$$\lambda(T) = 21.7 + 1.59 \cdot 10^{-2} T + 5.91 \cdot 10^{-6} T^2. \tag{2.8}$$

[7]PUREX stands for Plutonium and Uranium Recovery by EXtraction

Comparison of thermal conductivities depicted in Figure 2.9 clearly shows superior properties of metals in this respect.

Carbide fuels

High thermal conductivity and low concentration of light atoms leading to a hard neutron spectrum are the two most attractive features of carbide fuels. Instability especially at high temperatures, however, is the show stopper for carbide fuels.

Fabrication of carbide fuels is based on the following reaction when mono-carbide and sesqui-carbide are produced:

$$3UO_2 + 3PuO_2 + 16C \rightarrow (U, Pu)C + (U, Pu)_2C_3 + 12CO \tag{2.9}$$

Carbide powders are highly pyrophoric and cannot be handled in air. Instead, vacuum must be used during fabrication and that makes carbide fuel production very clumsy.

Fabrication in vacuum has also consequences for americium bearing carbide fuel. At low pressure americium carbide, AmC, dissociates already at the temperature of 1500 K. Most of americium would thus escape the fuel during fabrication. So far there is no solution to this problem and americium bearing carbide fuel cannot be produced.

The thermal conductivity of carbides is the strong point of this fuel. Coninck et al. suggested in their work the following empirical relationship for thermal conductivity of uranium carbide [34]

$$\lambda(T) = 19.5 + 3.57 \cdot 10^{-6} \left(T - 577\right). \tag{2.10}$$

Nitride fuels

Nitride fuels, such as carbide fuels, feature high thermal conductivity and low concentration of light atoms. Also fabrication of americium bearing nitride fuels is problematic, however still possible. Nitrides suffer from cost penalty compared to other fuels, because nitrogen used in fuel fabrication has to be enriched.

Industrial fabrication of uranium and plutonium nitrides is done similarly following the same process of reducing oxides

$$2UO_2 + 4C + N_2 \rightarrow 2UN + 4CO \tag{2.11}$$

It is difficult, however, to use the standard procedure when producing americium bearing nitride fuels. The reason is that americium nitride, AmN, has a tendency to dissociate into metallic americium and gaseous nitrogen during sintering. Sintering is used to increase pellet density and to ensure good mixing of nitrides. A possible solution is to use spark plasma sintering (SPS) instead of traditional sintering in a furnace. During SPS very high current runs through a pellet for a limited period

of time. Because the nitrides reach high temperatures only for a couple of minutes, dissociation of AmN should be minimized [35].

Natural nitrogen contains 99.634% of ^{14}N which could be transmuted into carbon in the following reaction

$$^{14}N + n \rightarrow ^{14} C + p. \tag{2.12}$$

Unfortunately, ^{14}C has very high radiotoxicity. To avoid unnecessary production of radiotoxic elements, nitrogen used in fabrication of nitride fuels must be enriched in ^{15}N. Isotopic enrichment is an expensive procedure requiring a lot of energy and massive use of nitride fuels becomes therefore expensive.

Because nitride fuels are rather hard, fuel-clad mechanical interaction as a consequence of extensive swelling must be avoided. There is a limited set of experimental data on swelling of nitride fuels at different temperatures. It appears that the irradiation temperature is more important for swelling of nitride fuels than the initial porosity [36]; further optimization of the irradiation conditions is therefore expected.

Thermal conductivity of nitride fuel depends on its composition, because the conductivity of uranium nitride is about twice as high as the conductivity of plutonium and americium nitrides. For nitride fuel without porosity the following empirical relations have been suggested [37, 38, 39]:

$$\lambda^{UN}(T) = 1.864T^{0.361} \tag{2.13}$$

$$\lambda^{PuN}(T) = 1.864T^{0.273} \tag{2.14}$$

$$\lambda^{AmN}(T) = 3T^{0.19} \tag{2.15}$$

Table 2.4: Summary of pros and cons of different fuel types.

	Oxide fuel	**Metallic alloy fuel**	**Carbide fuel**	**Nitride fuel**
Thermal conductivity	low	excellent	good	good
Swelling	OK	significant	OK	temperature dependent
Fabricability	OK	dust-free	problematic	expensive (enrichment)
Stability	good	very reactive	AmC dissociates	AmN dissociates
Neutron spectrum	softer	very hard	hard	hard

Chapter 3

Minor actinides in fast reactors

As indicated in Table 2.1, a standard LWR produces three minor actinide elements that are relatively abundant in the irradiated fuel: Np, Am and Cm. While separation of pure Np is not a problem, chemical similarity of Am and Cm with each other makes it difficult to separate them on an industrial scale. Unless there is progress in MA chemistry, Am and Cm have to be transmuted together. This chapter elaborates on challenges associated with introduction of minor actinides, especially Am and Np, into fast reactor fuel.

3.1 Doppler feedback

Critical reactors rely on a strict balance between neutron production and consumption. Every little distortion of such an equilibrium manifests in increase or decrease in power generation. It is a well-known fact that an increase in material temperature results in changes of the material neutron cross sections; cross section resonances observed in the epithermal energy region become wider and the probability for neutron interaction increases. The reactivity feedback associated with an increased fuel temperature is called the *Doppler feedback*. The name is derived from the Doppler effect known in acoustics; sound frequency registered by an observer depends on the speed of the observer and the source of the sound. In neutron physics, the material cross section as seen by the incoming neutron depends on the relative speed of the neutron to the material, i.e. on the vibration frequency of the atoms in the crystal lattice of the material - that is, in fact, on the material temperature.

In power-producing nuclear reactors the total Doppler feedback must always be negative. It means that with increased fuel temperature the increase of neutron cross section for capture must be steeper than the increase of fission cross section. An example of an isotope with a strong Doppler feedback is ^{244}Cm. Figure 3.1 shows that for ^{244}Cm the neutron capture cross section is the highest in the resonance

energy region; neutrons are captured predominantly there and any increase of the cross section in this region will have a significant impact on the neutron economy.

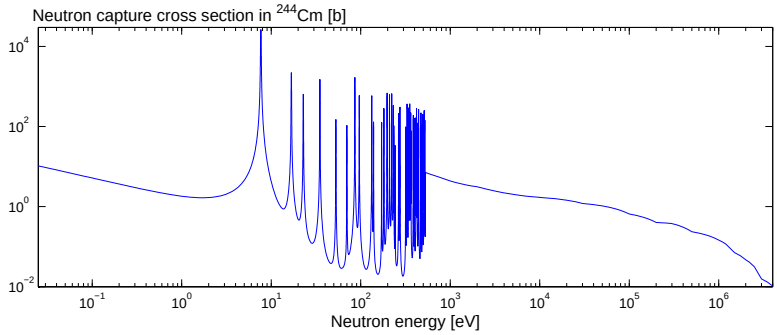

Figure 3.1: *Neutron capture cross section of ^{244}Cm from JEFF-3.1.1 nuclear data library [40].*

To quantify the Doppler feedback, *Doppler constant*, K_D, is frequently used. The Doppler constant is calculated as the difference between reactivity, ρ, at two different fuel temperatures, T_{fuel},

$$K_D = \frac{\rho_1 - \rho_2}{\ln \frac{T_2}{T_1}}. \tag{3.1}$$

A common unit of the Doppler constant is a Dollar (\$), which is the value of K_D / β_{eff}, where β_{eff} is the effective delayed neutron fraction.

When the temperature of a well-designed nuclear fuel increases, neutron capture increases due to the Doppler feedback, thus inhibiting the chain reaction. As a result, the power decreases and the temperature growth is halted. The change Doppler feedback coefficient is dependent upon the isotope in question and could be either positive (if a fission cross section is boosted) or negative (if a capture cross section increases instead). Figure 3.2 depicts the Doppler contribution to neutron capture in a standard MOX fuel, where ^{239}Pu stands for the most positive feedback while the presence of ^{238}U ensures that the total reactivity feedback remains negative.

Figure 3.3 shows that in a standard MOX fuel the Doppler feedback relies heavily on ^{238}U and one could believe that ^{238}U is unique in this respect. However, the same figure shows on the right hand side that ^{238}U stands for most of the Doppler feedback mainly because of its high concentration in the fuel compared to the other actinides. In fact, ^{240}Pu and ^{242}Pu could, in principle, offer a similar feedback. Their respective concentrations in the fuel, however, are usually much lower and so is their contribution to the total Doppler feedback.

Introduction of minor actinides into the fuel has a detrimental impact on the Doppler feedback. Figure 3.4 demonstrates that with, for example, Am in the core,

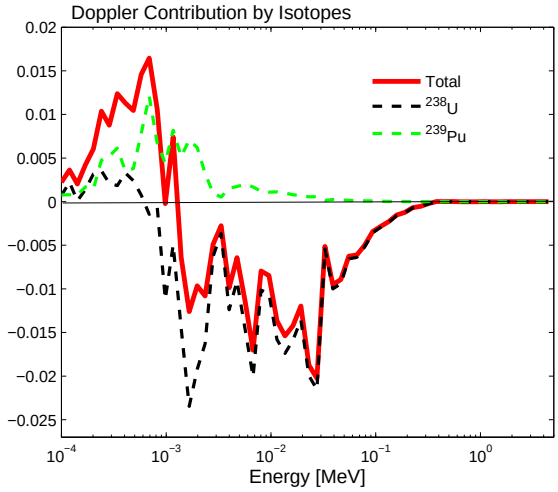

Figure 3.2: *The Doppler contribution to neutron capture (in red) is the difference in neutron capture after increasing the temperature from 300 K to 1800 K, here in standard MOX fuel loaded to SFR. The share of the two most prominent isotopes is shown in dashed lines. Notice that it is the 1-25 keV region that is crucial for the negative Doppler feedback.*

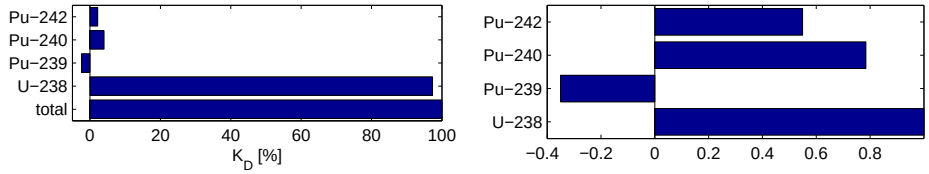

Figure 3.3: *Isotopic contribution to the Doppler feedback. To the left: relative contribution of the most prominent isotopes. To the right: contribution normalized to isotope concentration.*

fewer neutrons reach the softer part of the neutron spectrum. This reduction in neutrons reaching energies between 1 and 25 keV causes a weakening of the Doppler feedback, as fewer neutrons are available for capture in this crucial energy region. This phenomena is explained by the ^{241}Am neutron capture cross section. As depicted in Figure 3.5, ^{241}Am has a large neutron capture cross section, especially in lower energies, and thus many neutrons are thus absorbed in Am.

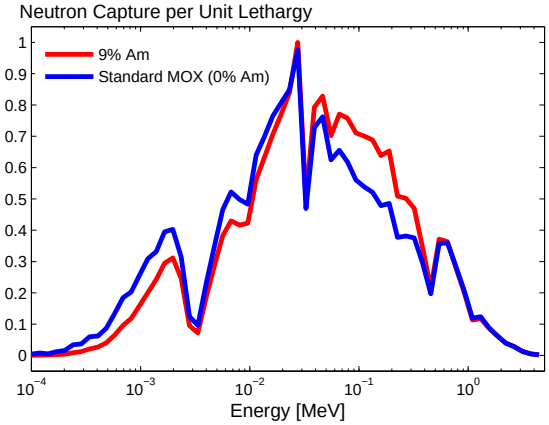

Figure 3.4: *Neutron capture in the fuel material of an SFR as a function of energy. Notice that with 9% of ^{241}Am more neutrons are captured at higher energy and consequently fewer neutrons reach the 1-25 keV region that is crucial for the Doppler feedback.*

One possibility to boost the Doppler feedback is to increase the coolant volume fraction by increasing the pin pitch. A higher coolant volume fraction results in increased neutron moderation and more neutrons will therefore be available for the Doppler feedback. Increasing the coolant volume fraction, however, is inadvisable for the following two reasons: First of all, in a Gen IV fast reactor the neutron spectrum should be as hard as possible. Secondly, as shown in Figure 3.6, the coolant volume fraction required for a significant increase of the Doppler feedback is unreasonably high.

As described above, introduction of Am to the core deteriorates the Doppler feedback. Figure 3.7 shows how the Doppler constant is decreased with increasing concentration of ^{241}Am; with 6% of Am in the core, the Doppler feedback is reduced by 50%. The trend is nearly identical for ^{243}Am and ^{237}Np.

3.2 Coolant temperature coefficient and coolant void worth

Aside from the Doppler feedback, the amount and density of the coolant also have a direct impact on the reactivity of fast reactors. Modifying the atomic density of

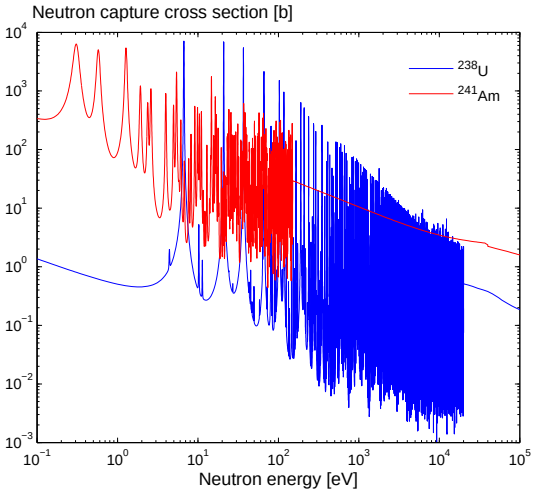

Figure 3.5: *Neutron capture cross section of* ^{241}Am *in comparison with* ^{238}U*. Data taken from JEFF-3.1.1 nuclear data library [40].*

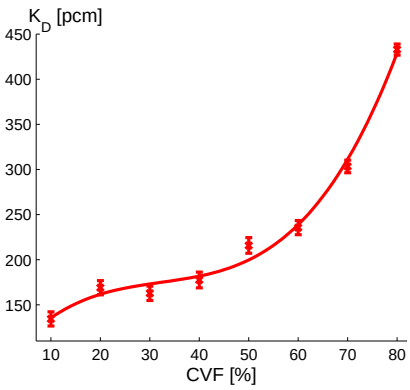

Figure 3.6: *The Doppler constant,* K_D*, as a function of coolant volume fraction,* CVF*, in an SFR.*

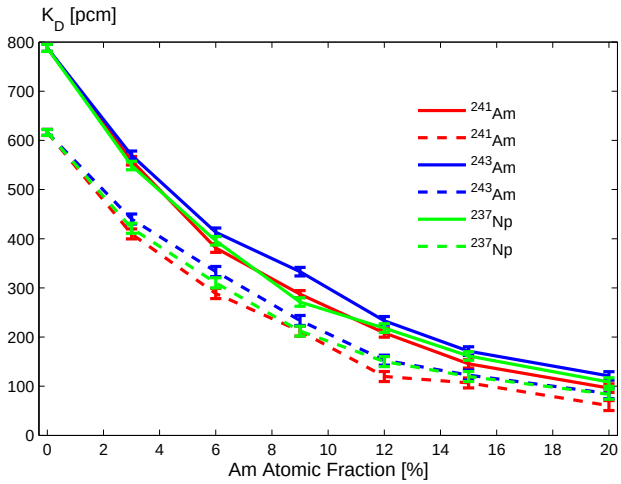

Figure 3.7: *The Doppler constant, K_D, as a function of increasing concentration of Am and Np in an SFR. The solid lines were calculated with JEFF-3.1 [41] and the dashed lines with ENDF/B-VI.8 [42] nuclear data libraries.*

the coolant results in a feedback which is a sum of two antagonistic components explained below: the leakage component and the spectral component.

The name of the leakage component comes from the neutrons leaving the core in axial or radial direction, because they are denoted as neutron leakage. Reduction of the coolant density opens more space for neutrons to escape the core with no or little interaction and results in higher leakage. The leakage component is always negative and becomes more dominant in smaller cores.

If the coolant density is reduced, the neutrons are consequently moderated to a lesser degree and the neutron spectrum becomes harder. In a harder spectrum, the number of fissions increases, because the fission probability of isotopes abundant in a typical FR fuel increases with neutron energy. The spectral component is therefore always positive and becomes predominant in larger cores.

The total coolant temperature coefficient is a sum of these two components and tends to be negative in smaller cores and positive in larger cores. Any temperature reactivity coefficient, α, is generally defined as the change of reactivity, ρ, with respect to the change of temperature, T. Hence the coolant temperature coefficient, $\alpha_{coolant}$, is quantitatively defined as

$$\alpha_{coolant} = \frac{\partial \rho}{\partial T_{coolant}}. \tag{3.2}$$

When minor actinides are added to the fuel, the leakage component remains

unchanged, but the spectral component increases. As depicted in Figure 3.8, the fission probability of, for example, ^{241}Am increases sharply with the energy of an absorbed neutron. The increase is more rapid and also starts in the lower, epithermal, energy region compared to ^{238}U. Because of this difference, coolant void worth does not grow with an increased concentration of ^{238}U in the fuel, unlike an increased concentration of ^{241}Am.

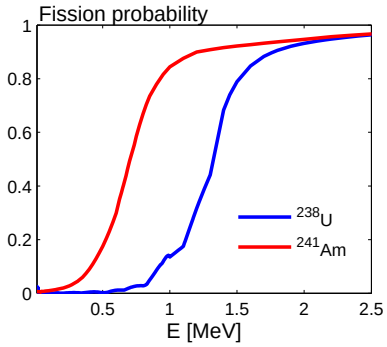

Figure 3.8: *Fission probability of ^{238}U and ^{241}Am. The data is retrieved from the JEFF-3.1.1 nuclear data library [40].*

The ultimate reduction of the coolant density is achieved by replacing the coolant by void. The *coolant void worth*, CVW, is defined as the difference between reactivities of the voided, ρ_{voided}, and standard, $\rho_{standard}$, cores,

$$CVW = \rho_{voided} - \rho_{standard}. \tag{3.3}$$

Figure 3.9 shows linear relationship between Am concentration in the fuel of the lead-cooled ELSY reactor design and the coolant void worth.

3.3 Effective delayed neutron fraction

Unlike prompt neutrons, which are produced directly (within 10^{-13} s) during the fission process, delayed neutrons are emitted with a time delay from decaying fission products. The delay depends on the half-life of the fission products and typically is in the range of seconds. The delayed neutrons are crucial for reactor control, because they relax the time frame of reactivity changes; instead of less than a microsecond, the time unit becomes seconds or minutes.

The delayed neutrons are born with lower energy compared to the prompt neutrons. Because the fission cross section of fissile isotopes decreases with energy, the fraction of delayed neutrons does not exactly correspond to the fraction of fissions induced by them. In well moderated cores, the delayed neutrons are more

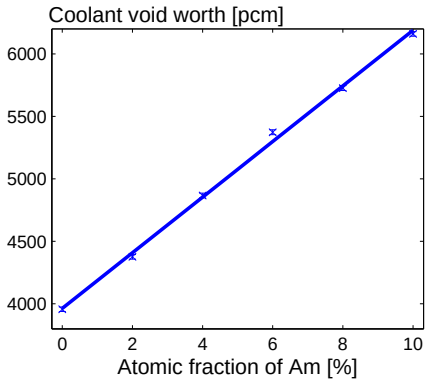

Figure 3.9: *Coolant void worth of the European Lead-cooled System (ELSY) loaded with nitride fuel increases linearly with the atomic fraction of* ^{241}Am.

efficient in inducing fission than the prompt neutrons, so the so-called *effective delayed neutron fraction* is usually higher than the simple delayed neutron fraction. The effective delayed neutron fraction is calculated by Monte Carlo codes as

$$\beta_{eff} = 1 - \frac{k_p}{k}, \tag{3.4}$$

where k_p is k_{inf} taking into account only prompt neutrons [43].

In general, the number of prompt neutrons increases with increasing mass number of isotopes that undergo fission, while the number of delayed-neutron emitters decreases. Because minor actinides have higher mass numbers than uranium, the introduction of minor actinides in the fuel decreases the delayed neutron fraction.

In addition to the lower delayed neutron fraction, the introduction of minor actinides to the core further reduces the effective delayed neutron fraction. As shown in Figure 3.5, ^{241}Am has a high neutron capture cross section at low energies, which is the typical energy of delayed neutrons. Hence the introduction of Am in the fuel reduces the effective delayed neutron fraction. This linear reduction is depicted in Figure 3.10 for the ELSY core loaded with nitride fuel.

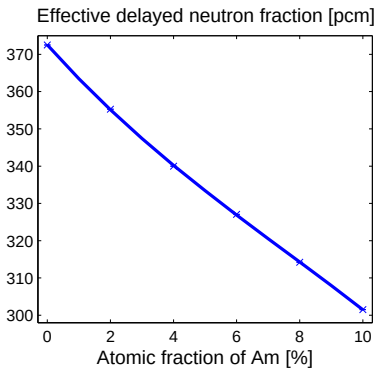

Figure 3.10: *Effective delayed neutron fraction of the ELSY core loaded with nitride fuel.*

Chapter 4

Calculation tools

In neutron physics, there are two general approaches to simulations: the deterministic and the stochastic. The physicist can either choose to follow the neutron on its average path (i.e. the deterministic approach) or to follow many neutrons on many different paths and obtain the result with a certain statistical uncertainty (i.e. the stochastic approach).

4.1 MCNPX

A popular particle transport codes used in nuclear reactor physics research is MCNP [44]. MCNP stands for Monte Carlo N-Particle transport code and it is a stochastic code which was originally developed by the Los Alamos National Laboratory (LANL) in the early seventies [45]. Since than, the code has been under a constant development and its latest and most advanced version is called MCNPX (where X stands for eXtended). MCNPX is capable of simulating 34 particle types and more than 2000 heavy ions at low, medium and very high energies. Data libraries containing particle-interaction can be replaced by physics models if the libraries are not available.

It is the versatility and long-lasting active support that make the code unique and popular. In recent years, however, MCNPX suffers from tough license conditions as opposed to older versions of MCNP which used to be actively distributed among the scientific community by LANL.

MCNPX is a powerful tool which can calculate many different parameters, but it is always up to the user to ask the right question. To ask a question, MCNPX uses so called *tallies*. A tally can be explained as a count or record and it is a piece of information MCNPX stores during particle transport through the geometry, i.e. through surfaces defining cells which make up the geometry. As shown in Table 4.1, there are nine different tallies in MCNPX.

In **Paper I** MCNP 5 [46] was used and in **Paper II** MCNPX 2.7.A [47] was utilized. The data libraries were used up to their maximum energies and models

Table 4.1: Tallies available in MCNPX.

Tally Code	Tally Description
F1	Current integrated over a surface
F2	Flux averaged over a surface
F4	Flux averaged over a cell
F5	Flux at a point or ring detector
F6	Energy deposition averaged over a cell
+F6	Collision heat
F7	Fission energy deposition averaged over a cell
F8	Energy distribution of pulses created in a detector by radiation
+F8	Charge deposition

were used for higher energies. Tallies F1, F4 and F8 were widely used. The F1 tally counts particles passing a given surface and represents the basic tally in MCNP. On the other hand, the pulse height tally, F8, is a new advanced tally which was not included in the earlier versions of MCNP and appeared only in MCNPX.

4.2 Serpent

For calculation of burnup and reactivity-related feedbacks a relatively new Monte Carlo code called Serpent was used in **Paper III** and **Paper IV** [48]. Serpent is a continuous-energy stochastic code that utilizes the Woodcock delta-tracking [49] instead of the more traditional surface-to-surface particle tracking. As a consequence, Serpent is 2-13 times faster for fast reactor calculations compared to MCNP [50]. In this work we used Serpent in its version 1.1.14 and 1.1.16 [51] together with the JEFF-3.1 nuclear data library [41].

Besides the significant speed-up factor, Serpent has also other advantages compared to MCNP. One of them is the ease of the license agreement which is granted to the whole university as compared to personal licenses for MCNP. The disadvantage of Serpent is its youth resulting in simplicity and lack of advanced functions. At the moment a more advanced version of Super Serpent (also called Serpent 2) is in beta testing and a full release is expected in 2012. Super Serpent is a new and re-written version with focus on memory management and parallelization. It also serves as the development platform for new capabilities, such as gamma transport and multi-physics [52].

4.3 SAS4/SASSYS

Transient calculations for **Paper III** and **Paper IV** have been performed by Reactor Dynamics and Safety Analysis System SAS4A/SASSYS version 3.1 [53]. The purpose of the code is deterministic analysis of the initiating phases of hypothetical

accidents in liquid metal cooled fast reactors. The original code was developed for SFR with oxide fuel, but later the capabilities have been extended to include lead-cooled systems. SAS4A consists of several modules that pass data to each other: thermal dynamic & thermal hydraulic, estimation of failure criteria, geometrical model of the primary loop and the point kinetic model for calculation of reactivity variation due to evolution of core characteristics in time. On one hand, SAS4 is focused mainly on the primary circuit and feedbacks from the secondary circuit play a secondary role. On the other hand, compared to "system codes" such as e.g. RELAP5, SAS4 does not suffer from numerical instability problems and is thus more suitable for simulation of the very first moments of the transients, when the feedback from the secondary circuit has not yet reached the core anyway.

Chapter 5

Experimental set-ups

This chapter describes experimental set-ups that have been used or simulated in the thesis. Experiments for **Paper I** were performed at YALINA-Booster, the SCANDAL set-up was simulated in **Paper II** and oxide and nitride versions of ELSY were studied in **Paper III** and **Paper IV**.

5.1 YALINA-Booster

The YALINA experiments performed at the Joint Institute for Power and Nuclear Research in Sosny, outside Minsk in Belarus, started at the beginning of this millennium by an experiment called YALINA-Thermal. The well-moderated neutron thermal spectrum inside polyethylene was soon replaced by a harder spectrum and in 2005 another set-up especially designed for a harder spectrum was constructed in the same room.

The YALINA-Booster facility is a two-zone subcritical core coupled to a neutron source. The inner fast zone (called also the booster zone) is closely packed to the neutron source while the thermal zone surrounds the fast zone.

The neutron source employs the fusion reaction between accelerated deuterons and a target containing tritium, providing neutrons with energy around 14 MeV. The subcriticality of the investigated configuration was $k_{eff} = 0.98410 \pm 0.00008$ (calculated by MCNP5 using the JEFF-3.1.1 neutron library [40]).

Both the thermal and the booster zones contain axial experimental channels. There are four experimental channels in the booster zone, three channels in the thermal zone and three channels in the reflector (two axial and one radial). A vertical cross section of the core is given in Figure 5.1.

The standard full-sized booster zone (as of February 2006) was composed of a lead lattice and consisted of two parts with two different enrichments of fuel pins. The inner part closest to the target contained 132 fuel pins made of metallic uranium with 90% enrichment in ^{235}U. The outer part contained 563 fuel pins with uranium dioxide enriched to 36%.

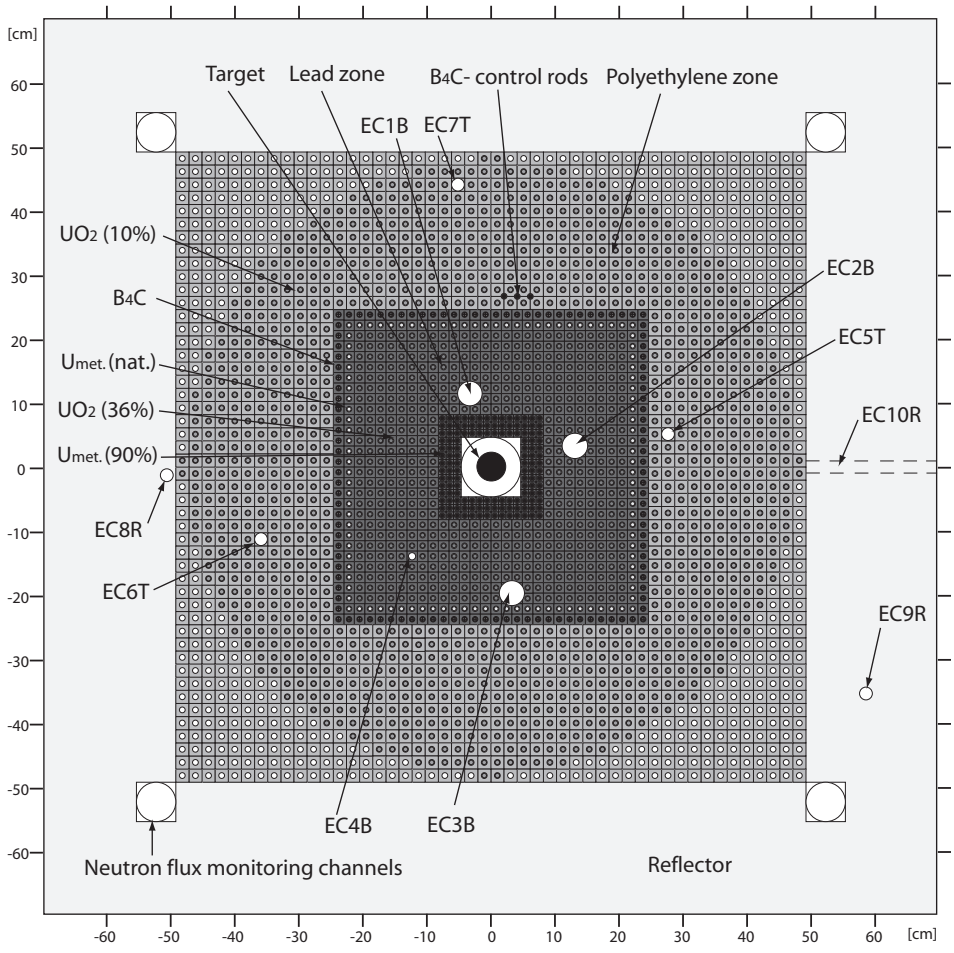

Figure 5.1: *Vertical cross section of the YALINA-Booster core.*

The two outermost rod layers in the fast zone form a thermal neutron filter. The filter is transparent to fast neutrons, but it absorbs thermal neutrons penetrating into the booster zone from the thermal zone. The filter consists of one layer of fuel rods made of natural uranium and one layer of rods filled with boron carbide, B_4C. The natural uranium absorbs neutrons and emits instead fast fission neutrons. The boron serves as a neutron absorber.

The thermal zone has a polyethylene lattice in cylindrical geometry with EK-10 fuel pins made of uranium dioxide enriched to 10%. There is also a possibility of inserting three B_4C control rods in the thermal zone.

5.2 The SCANDAL set-up

The history of the SCANDAL set-up (SCAttered Nucleon Detection AssembLy) dates eleven years back to 2001. It was constructed for detection of scattered neutrons in the 50 - 130 MeV energy interval [54]. Since then, SCANDAL has had a significant contribution to nuclear data libraries in the mid-energy region [55, 56, 57, 58]. Later, the set-up was upgraded to detect neutrons up to 175 MeV [59].

Protons accelerated to 179.3 ± 0.8 MeV by the Gustaf Werner cyclotron [60] impinge on a neutron production facility [61] at The Svedberg Laboratory (TSL) in Uppsala, Sweden. The facility utilizes (among others) a 23.5 mm thick lithium target, enriched to 99.99% in ^{7}Li, and the ^{7}Li(p,n)^{7}Be reaction to create a quasi-monoenergetic neutron spectrum consisting of a high-energy peak and a low-energy tail [62] (see Figure 5.2). The average neutron energy in the peak is 175.0 MeV and the width of the peak is approximately 5 MeV. The peak contains about 40% of all neutrons. A neutron beam is formed by a set of collimators and creates a circular beam spot with a diameter of 8.2 cm at the scattering target position (the diameter can vary depending on the collimator set). In a typical run, before reaching the scattering target, the neutron beam would pass another experimental set-up called Medley [63] as depicted in Figure 5.3. Medley, however, only has a negligible influence on the beam since its target is less than 0.5 mm thick.

The SCANDAL set-up consists of two arms that can be rotated around a pivot point where the scattering target is located. Both arms are geometrically identical. Each arm is equipped with four plastic scintillators: a veto, a converter and triggers 1&2. The veto and both triggers consist of 2 mm thick plastic scintillators. The veto is used for fast charged-particle rejection, so in a standard neutron detection mode, a trigger condition to read out the system consists of a coincidence between the triggers 1&2 vetoed by the front plastic scintillator. Since it is not possible to detect neutrons directly, conversion to a charged particle (e.g. a proton) is necessary. The neutron-to-proton converter in SCANDAL is a 20 mm thick plastic scintillator ($C_1H_{1.102}$). Using an active converter allows the proton energy loss within the converter to be measured and compensated for. An array of eight scintillators at the back side of each arm is intended to stop the protons so that their full energy is

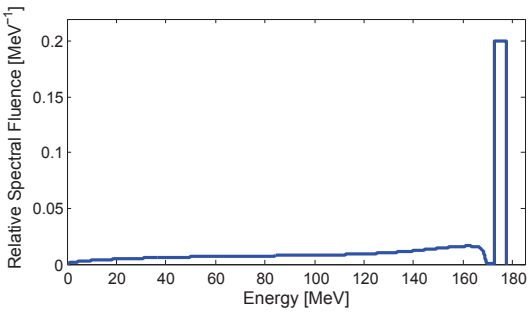

Figure 5.2: *Spectrum of the quasi-monoenergetic neutron beam at TSL [62]. The full energy peak contains about 40% of the neutrons.*

deposited. The scintillators are 9 cm deep, 8 cm wide and 22 cm high crystals made of cesium-iodine doped with sodium, CsI(Na). They are counted from the left as CsI 1 to CsI 8 on the left arm and CsI 9 to CsI 16 on the right arm. Two drift chambers are positioned between triggers 1&2 at both arms. The drift chambers provide information about proton trajectories, so the neutron-to-proton conversion point inside the converter can be determined and simply related to the scattering angle of the original neutron. The spatial disposition of the scintillators and the drift chambers is depicted in Figure 5.3.

Another arrangement including a so called *multitarget* box is used for calibration. The box is located about one meter upstream compared to the standard target position and contains a set of thin (~1 mm) carbon and polyethylene targets. Although only the hydrogen in the plastic material is required for the calibration, plastic material is used for practical reasons. The carbon contribution can, however, be subtracted using the signal from the pure carbon layers. Multi-wire proportional counters in between different multitarget layers facilitate distinction of the plane where the neutron-to-proton conversion occurred. In the proton mode used for calibration, the data acquisition trigger consists of a triple coincidence between the veto and trigger detectors 1&2.

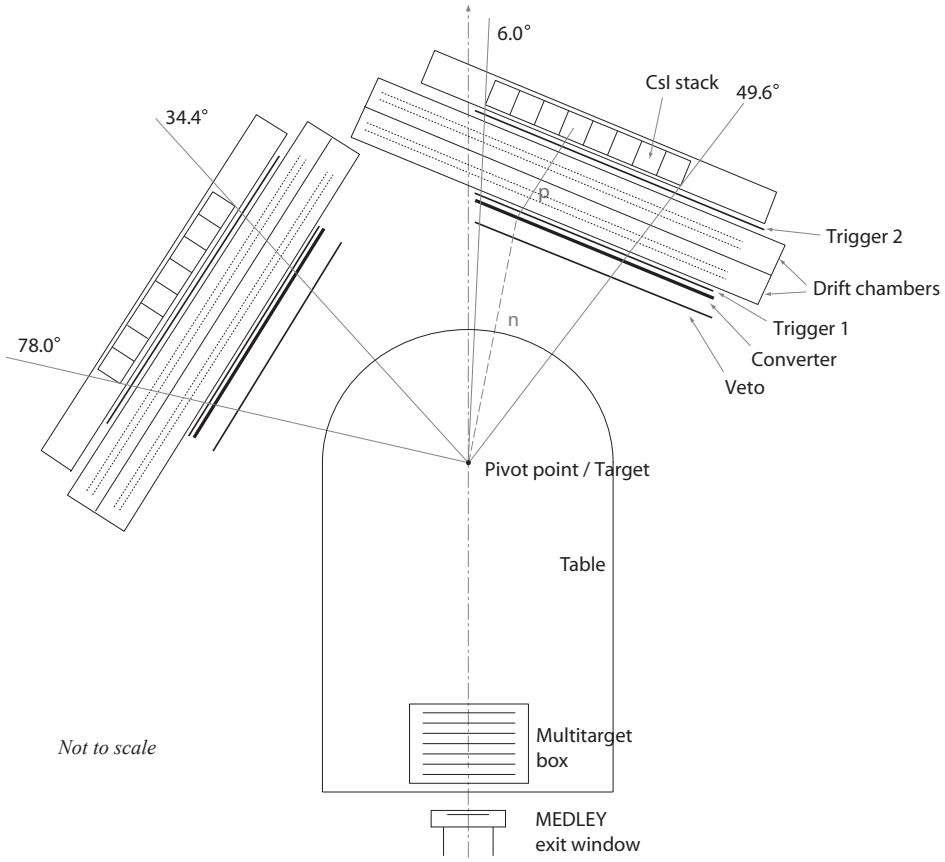

Figure 5.3: *Schematic view of the SCANDAL set-up in one of the configurations. Here the right arm is as close as possible to the beam with CsI 9 yet outside the beam.*

5.3 ELSY

The European Lead-cooled SYstem (ELSY) was developed within the Sixth Framework Program of EUROATOM (FP6) and its goal was to present a conceptual design of a lead-cooled fast reactor that could fully comply with the Gen IV objectives. The project was successfully finished in 2010 and is now followed in FP7 by the LEADER project (LEad-cooled European Advanced DEmonstrator Reactor), which aims to present a ready-to-build design of ALFRED - the Advanced Lead Fast REactor Demonstrator.

ELSY is a pool-type lead-cooled fast reactor with a thermal power of 1500 MW_t. The reference subassembly design is open square and the fuel is MOX mixed with minor actinides. Details of the ELSY reference design are summarized in Table 5.1 [64] and also elaborated by Allemberti et al. [65].

Table 5.1: Basic parameters of the ELSY reference design.

Fuel type	MOX
Subassembly type	open square
Thermal power	1500 MW_t
Electrical power	600 MW_e
Cladding material	T91
Core inlet temperature	400°C
Core outlet temperature	480°C
Vessel inner diameter	577 cm
Fuel pin active height	90 cm
Upper plenum height	121 cm
Lower plenum height	113.3 cm
Number of SA	162
Number of fuel pins per SA	428
Fuel outer diameter	4.45 mm
Number of control rods	8

The reference design of ELSY contains oxide fuel and that is the core studied in **Paper III**. In **Paper IV** a similar core is used but this time loaded with nitride fuel. The cores are not exactly identical, some geometrical differences are obvious from Figure 5.4.

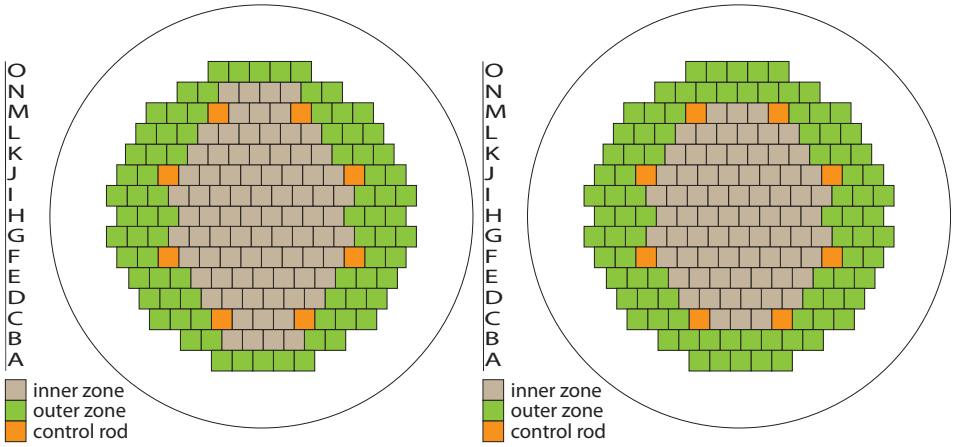

Figure 5.4: *Cross section of the ELSY cores. Oxide fuel to the left and nitride fuel to the right hand side. Both cores include the inner and the outer zones and also eight control rods.*

Chapter 6

Neutron detection and cross-section measurements

The neutron is a neutral and non-ionizing particle which cannot be detected directly. The neutron can only be seen indirectly after it undergoes a nuclear reaction or scattering resulting in a charged, directly detectable secondary particle or γ-radiation. The following paragraphs describe the five most common neutron detection methods.

Charged particle production

The neutron can hit a target nucleus and produce a charged particle, for example an α-particle. The charged particle is detected as an evidence of the reaction and thus as an evidence of the neutron presence. The following example is very common for detection of thermal neutrons.

$$^{10}_{5}B +^{1}_{0} n \rightarrow^{7}_{3} Li^{*} +^{4}_{2} \alpha \qquad\qquad Q = 2.310\ MeV \tag{6.1}$$

Fission chamber

A fission chamber contains fissile material and the neutron fission the material producing fission fragments. The fission fragments have very high momentum and can for example ionize gas in a gas detector. Fission chambers are widely used in nuclear reactor physics. Their sensitivity depends on the fissile material which is often ^{235}U, ^{238}U or ^{239}Pu.

Thermoluminescent dosimeters

Tablets of a luminescent material are often kept by nuclear staff in personal dosimeters. When the tablets are heated up, luminescent light is released. The intensity of the light is proportional to the neutron dose. This detection method provides

results only with a certain delay which could be a significant drawback in some experiments.

Neutron activation analysis

Small thin foils made of different materials are exposed to a neutron flux, the neutrons cause nuclear reactions in the foils resulting in unstable products. The foils become so called *activated* and start to decay. γ-radiation released during the decay is proportional to the neutron flux and can be measured later. Energy sensitivity can be adjusted by the choice of irradiated material and both thermal and fast neutrons can be detected.

Proton recoil

Proton recoil is a special case of production of a charged particle and is frequently used for higher energies. In principle, any isotope can be used as a target bombarded by fast neutrons which would push an easily detectable proton out of the nucleus. On the other hand, all isotopes (except for hydrogen) have a non-zero Q-value of such a recoil which makes hydrogen the most suitable target material.

Probability of a specific neutron-nucleus reaction is given by the corresponding neutron cross section, however, to measure neutron cross section, the neutrons have to be detected. It means they have to undergo a nuclear reaction with a known cross section. And this is the problem of circular reasoning with neutron cross section measurement. It seems we need to know the cross section in order to be able to measure it. Fortunately, there are possible solutions to this stalemate. The following sections present solutions focused on fast neutron detection, using a collimated neutron beam as that is the interesting case in this work.

Neutron detection, however, is only the first step towards the neutron cross section measurements. The following four sections elaborate on particular techniques applicable for neutron elastic scattering cross section measurements.

6.1 The tagging technique

The neutrons originated in nuclear reactions are often accompanied by other particles. If the associated particle is known and easily detectable, it can be used for reaction tagging. If there is only one reaction product besides the neutron and the energy of the product is measured, the neutron energy can be derived. For a relatively high precision, this method would typically be used as a reference measurement. On the other hand, intensity of the beam is limited. The following

example is a reaction often utilized in spallation neutron sources in reactor physics experiments and the tagging particle in this case is ${}^{3}_{2}He$.

$$ {}^{2}_{1}D + {}^{2}_{1}D \longrightarrow {}^{3}_{2}He + n \qquad\qquad Q = 3.27\ MeV \tag{6.2} $$

6.2 The case of hydrogen

The advantage of hydrogen in the mid-energy region is its limited variety of only three possible reactions with the neutron: (n,p) elastic scattering (99% of the total cross section), ${}^{1}_{1}$H(n,γ)${}^{2}_{1}$D neutron capture and bremsstrahlung, (np,npγ). When a neutron collides with the ${}^{1}_{1}H$ hydrogen atom (i.e. a proton), then the proton starts to move. Using minor corrections for the other two reaction channels, the (n,p) reaction can be supposed to be the only reaction. In that case, to measure the cross section means to measure the total cross section. The total cross section could be easily determined from the transmission ratio, as depicted in Figure 6.1.

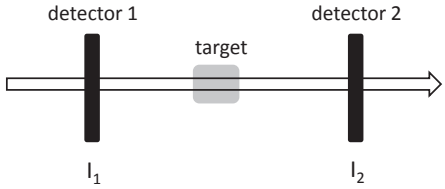

Figure 6.1: *Schematic view of the transmission technique for total cross section measurement.*

A neutron beam of a known intensity, I_1, passes through a relatively thin target and undisturbed neutrons of beam intensity I_2 are detected by a neutron-sensitive detector. With a known target thickness, x, the total macroscopic cross section, Σ_{tot}, can be calculated using

$$ \frac{I_2}{I_1} = e^{-\Sigma_{tot}x}. \tag{6.3} $$

The accuracy can be improved by increasing the distance between the target and the detector, so that neutrons scattered on the target are not detected.

The total neutron scattering cross section is the first step. Often it is useful to have differential cross sections for different angles. The following equipment depicted in Figure 6.2 can be used to measure the differential cross section for neutrons scattered on hydrogen.

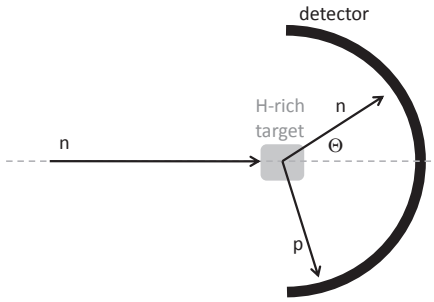

Figure 6.2: *Schematic view of the experimental layout for differential cross section measurements. The detector is a position-sensitive neutron detector.*

The angle-integrated differential cross section, $\frac{d\sigma}{d\Omega}$ from the detector in Figure 6.2 can be normalized to the known total cross section, σ_{tot} as

$$\sigma_{tot} = \int_0^{2\pi} \frac{d\sigma}{d\Omega}\, d\Omega = 2\pi \int_{0^\circ}^{180^\circ} \frac{d\sigma}{d\Omega} sin\Theta\, d\Theta \tag{6.4}$$

6.3 The new reaction cross section approach

The situation becomes more complicated when the variety of possible reaction channels grows. In such a case, it would be desirable to utilize the approach as depicted in Figure 6.1 and somehow subtract all interactions apart from neutron elastic scattering. If the elastic scattering cross section, σ_{el}, is subtracted from the total cross section, σ_{tot}, the so called *reaction cross section*, σ_{r} is obtained as

$$\sigma_r = \sigma_{tot} - \sigma_{el}. \tag{6.5}$$

If for the variety of possible reactions it appears difficult to measure the reaction cross section, the elastic cross section could be measured directly, using the layout depicted in figure 6.3. An array of neutron sensitive, high energy resolution detectors would be able to select only elastically scattered neutrons according to simple kinetics, namely according to their energy and scattering angles.

This measurement provides also data for inelastic scattering cross section as a special case of the reaction cross section. The untouched neutrons, $\mathrm{I_{ut}}$, which have not interacted with the target and which kept their energy and zero scattering angle, could be subtracted from the original beam intensity, $\mathrm{I_0}$, together with the elastically scattered neutrons, $\mathrm{I_{el}}$, to obtain the number of inelastically scattered neutrons, $\mathrm{I_{in}}$. So the number of inelastically scattered neutrons, $\mathrm{I_{in}}$, becomes

$$I_{in} = I_0 - (I_{ut} + I_{el})\,. \tag{6.6}$$

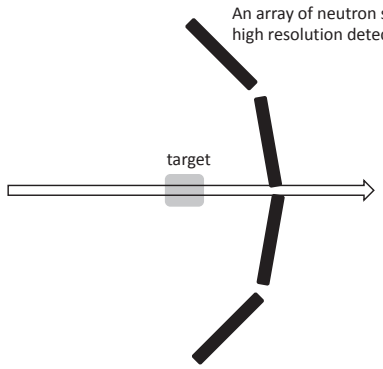

Figure 6.3: *Schematic view of the experimental layout for measurement of scattered neutrons.*

6.4 The improved reaction cross section approach

Sometimes it is not possible or desired to place the detectors close to the target. Alternatively the spatial resolution of the detector array is too low and there is a need for additional equipment which would not fit between the target and the array as they are indicated in Figure 6.3. In that case, a so called *converter* could be used to convert scattered neutrons into protons which are detected further away. To be able to distinguish elastically and inelastically scattered neutrons based on their energy, the neutron-to-proton conversion must be energetically unambiguous (i.e. without production of excited states) and the proton energy has to be measured.

The proton energy could be measured in several ways.

- The **time of flight method** (TOF) takes advantage of the known distance the particles have to travel from an accelerator to the detector. Using a precise clock, it is possible to calculate the particle velocity and thus the energy. The TOF technique, however, is not practical for very high energy neutrons. A typical limit is 25 MeV. For example, at the energy of 25 MeV a proton would travel 20 m within less than 30 μs.

- Another option is to use a **bending magnet**. Because all protons have the same mass, their trajectories would bend in a magnetic field and sort the protons by their velocity. Such a measurement would be precise, but costly.

- The most affordable option at high energies is using **large detectors** where the protons would stop and deposit all the energy. In this respect, crystals of inorganic scintillators appear to be a good choice. For example, to fully stop a proton with 200 MeV it is necessary to use more than 8 cm of a typical scintillator material CsI.

The only energetically unambiguous converter material is pure hydrogen, which is technically difficult to handle for its explosibility and physically non-ideal due to its low density. The target could, however, be made of a hydrogen-rich material and reactions on the additional elements have to be singled out. Typically the hydrogen rich material would be plastics which also contains carbon. The carbon contribution could be measured separately using a pure carbon target and subtracted afterwards. A more advanced approach to separate protons converted on hydrogen and carbon utilizes the energy difference between protons created on carbon and hydrogen. The Q-value for proton recoil on hydrogen is zero, while the Q-value of the ^{12}C(n,p)^{12}B reaction is -12.6 MeV. Protons converted at hydrogen have thus energy higher at least by 12.6 MeV compared to protons converted on carbon at the same angle.

For the neutron elastic cross section measurement at 175 MeV a dedicated set-up with a number of additional triggers and other background-filtering gadgets has to be used. Such a set-up based on the improved reaction cross section approach is described in the following section.

Chapter 7

Discussion of results and conclusions

This thesis presents americium as one of the most troublesome byproducts of nuclear power. It shows that the other byproducts produced in a fission reactor are either not as dangerous or decay relatively quickly. Americium requires special treatment also due to its behavior in the core of a fast reactor; it has a detrimental effect on vital safety parameters, namely the Doppler feedback, effective delayed neutron fraction and coolant void worth. This work approaches americium transmutation from two different points of view: firstly, by providing nuclear data necessary for simulations of americium-burning facilities and by discussing approaches and tools for effective simulations. Secondly, by looking for the maximum concentration of americium allowed in the fuel of ELSY.

A popular tool for neutronic Monte Carlo simulations is MCNP. In **Paper I**, MCNP calculations are compared with experimental results obtained by foil activation. Foil activation represents a method with an excellent combination of simplicity and reliability. In fact, there are not so many other ways of obtaining experimental characteristics of neutron spectrum that could easily be simulated by MCNP directly.

As we expected, MCNP was not able to predict the neutron spectra-dependent reaction rates precisely, especially for high threshold reactions. We performed an uncertainty analysis in order to identify possible reasons for that discrepancy. The uncertainty level, however, remained smaller than the observed differences. Based on that we were able to confirm that MCNP has difficulties to predict behavior of subcritical systems, especially in the fast neutron energy region. This conclusion is important, because neutron transport is a fundamental task of MCNP and the neutron flux is a fundamental variable which is used for calculation of many other variables.

During the analysis, we also identified an incorrect cross section in the CENDL-3.1 library. The discovery is of high importance, because the $^{115}In(n,\gamma)^{116}In^{m}$

reaction is often used in neutron activation as a monitor reaction.

For MCNP critical calculations, it is necessary to supply libraries with neutron cross sections. The objective of the SCANDAL experiment was to measure neutron scattering cross sections at energies that are less common in critical cores, but appear, for example, in accelerator-driven systems. **Paper II**, as a part of the SCANDAL cooperation, lists a number of rather technical parameters that are useful for analysis of the obtained experimental data.

Another Monte Carlo code, namely SERPENT, has been used in **Paper V** to show that pin-cell model of a LFR loaded with nitride fuel should not be used for calculation of the Doppler effect, because it is not conservative. The paper shows that due to the positive Doppler feedback on the outskirt of the core, the full-core calculation exhibits a lower Doppler feedback than calculated by a corresponding pin-cell model.

Direct disposal of americium by transmutation in a fast reactor is discussed in **Papers III and IV**. The papers present a parametric study aiming at finding the maximal amount of americium that can be safely loaded into a lead-cooled fast reactor.

In **Paper III** the reference design of the European Lead-cooled SYstem ELSY is analyzed. The analysis revealed that, on one hand, during the ULOF transient with any investigated americium concentration there is no violation of the temperature limits. On the other hand, during the UTOP transient, the fuel temperature limit is exceeded for any significant concentration. As a consequence, we conclude that the reference ELSY design is not suitable for americium transmutation.

The purpose of **Paper IV** is to suggest a modified ELSY design that could be more suitable for Am transmutation. Due to its high thermal conductivity, nitride fuel is used instead of oxide fuel and the core volume is reduced. This modified ELSY design manages up to 8% of Am during ULOF. During UTOP at EOC, however, the maximal allowed cladding temperature is exceeded with fuel containing any additionall Am. Thus the modified design can be used for Am transmutation only with a power penalty of 4% for each per cent of Am. This penalty is higher than that reported for SFR.

Appendix A

Concluding remarks

The following chapter sets the publications included in the thesis in a broader context.

A.1 Paper I

More than seldom physicists proudly distinguish two categories of researchers: the experimentalists as opposed to the theoreticians. The experimentalists often claim that they are doing the "real" science, because they study directly the behavior of the Mother Nature. On the other hand, the theoreticians often look down upon the experimentalists, who are left with many limitations imposed on them by practicalities.

The objective of **Paper I** was to confront these two worlds: MCNP as the de facto standard of reactor-physics Monte Carlo simulations was confronted with results obtained experimentally. The area of application was set to accelerator driven subcritical systems, where other authors have previously observed MCNP in difficulties.

A.2 Paper II

The group of Applied Nuclear Physics at the Uppsala University is well known for its contributions to the world of nuclear data. Experimental measurements of double-differential cross sections for a variety of particles and targets have been conveniently performed at the Svedberg laboratory located in the historical center of Uppsala. The vicinity of experimental facility to the staff preparing, performing and analyzing experimental campaigns, has surely contributed to the efficiency of obtaining the experimental results.

The SCANDAL experiment that was originally developed at the beginning of this century, was refurbished, modernized and upgraded to handle higher energies. During two experimental campaigns using the upgraded SCANDAL, new data was

obtained for neutron scattering cross sections of bismuth, iron and silicon. The experiments were held so that both elastic and inelastic scattering cross sections could be extracted from the data.

The simulation effort which resulted in **Paper II** was focused on supporting the off-line data analysis that was to come after the experiment. A number of useful parameters have been calculated which enabled a deeper insight in the experimental procedure and physics behind. Unfortunately, in spite of this extensive support, it turned out that the data could not be analyzed because of a very low signal-to-noise ratio. The effort to overcome this problem was interrupted in 2010 together with the employment contract of the responsible PhD student. At the moment, the data is frozen and there is no analysis foreseen in the near future.

A.3 Paper III

The European research on fast reactors has been mainly focused on sodium-cooled reactors (SFR) with France as the leader. The SFR technology has already been demonstrated and construction of the Astrid prototype is expected in the next decade. Lead-cooled technology has been chosen as a back up option, in case sodium reactors would not be able to reach the desired industrial deployment. Within the lead community, it is Italy that takes the most significant portion of initiative.

On its way to build the first demonstrator, the lead-community made an exercise in design and developed the European Lead-cooled SYstem (ELSY). The objective of the exercise was to prove that it is in principle possible to design a lead-cooled reactor that fully complies with the Gen IV objectives.

While ELSY does comply with the Gen IV sustainability requirement to "Reduce the amount of long-term radiotoxic irradiated fuel", it was interesting to investigate whether ELSY could do even more. In **Paper III** we load additional americium to the ELSY core and examine the impact on its safety. Instead of a simple check of the relevant reactor coefficients, we decided to perform a real transient analysis of the core.

A.4 Paper IV

The result of **Paper III**, namely the fact that the reference ELSY design cannot be used for effective Am transmutation, was a surprise. It has been therefore decided to modify the design and hopefully reach another, possibly less conventional design that would be suitable for Am transmutation. The choice was made for nitride fuel.

The possibility to use nitride fuel was examined already during the ELSY project. Nitride fuel has some important properties superior to oxide fuels. There are even some indications that in future, nitride fuel could really be loaded to traditional LWRs.

A.5 Paper V

At the Reactor Physics group at KTH for quick estimates and teaching we have been using a simplified pin-cell model instead of a full-core model in Monte Carlo calculations. There has always been the question: "How accurate is that?" **Paper V** is, in fact, a byproduct of some other activities dedicated to the Doppler feedback. It became necessary to investigate deeper the error introduced by the simplification. The choice of coolant, fuel composition and core geometry is directly related to NELSY and the work on the Doppler Feedback.

References

[1] P. Karkanas, R. Shahack-Gross, A. Ayalon, M. Bar-Matthews, R. Barkai, A. Frumkin, A. Gopher, and M. Stiner, "Evidence for habitual use of fire at the end of the Lower Paleolithic: Site-formation processes at Qesem Cave, Israel," *Journal of human evolution*, vol. 53, no. 2, pp. 197–212, 2007.

[2] EIA, *International Energy Outlook 2011*. Washington: U.S. Energy Information Administration, 2011.

[3] P. D. Jones, T. J. Osborn, and K. R. Briffa, "Global monthly and annual temperature anomalies, 1850-2010," Retrieved in January 2012. `http://cdiac.ornl.gov/ftp/trends/temp/jonescru/global.txt`.

[4] A. Neftel, H. Friedli, E. Moor, H. Lotscher, H. Oeschger, U. Siegenthaler, and B. Stauffer, "A compendium of data on global change: Historical CO_2 record from the siple station ice core," tech. rep., ORNL/CDIAC-65, Oak Ridge National Laboratory, Oak Ridge, Tenn., U.S.A., 1994.

[5] U.S. Department of Commerce, National Oceanic and Atmospheric Administration, Global Monitory Division, "Maona Loa data," Retrieved in January 2012. `http://www.esrl.noaa.gov`.

[6] R. Watson and the Core Writing Team (eds.), *Climate Change 2001: Synthesis Report. A Contribution of Working Groups I, II, and III to the Third Assessment Report of the Integovernmental Panel on Climate Change*. Cambridge, United Kingdom, and New York, NY, USA: Cambridge University Press, 2001.

[7] G. Marland, T. A. Boden, and R. J. Andres, "A compendium of data on global change: Global, regional, and national CO_2 emissions," tech. rep., Carbon Dioxide Information Analysis Center, Oak Ridge National Laboratory, Oak Ridge, Tenn., U.S.A., 2007.

[8] J. T. Kiehl and K. E. Trenberth, "Earth's Annual Global Mean Energy Budget," *Bulletin of the American Meteorological Society*, vol. 78, pp. 197–197, Feb. 1997.

[9] D. Weisser, "A guide to life-cycle greenhouse gas (GHG) emissions from electric supply technologies," *Energy*, vol. 32, no. 9, pp. 1543 – 1559, 2007.

[10] Vattenfall, "Life-cycle assessment, Vattenfall's electricity in Sweden," tech. rep., Vattenfall Business Service Nordic AB, 2005.

[11] International Atomic Energy Agency (IAEA), "Power reactor information system," Retrieved in May 2012. http://www.iaea.org/programmes/a2/.

[12] OECD/NEA, "Actinide and fission product partitioning and transmutation; Status and assessment report," tech. rep., Nuclear Energy Agency, NEA, Paris, France, 1999. NEA01507, Annex E.

[13] ICRP, "Age dependent doses to members of the public from intake of radionuclides: Part 5, Compilation of ingestion and inhalation dose coefficients," tech. rep., International Comission on Radiological Protection, ICRP, 1996. ICRP Publication 72.

[14] G. Youinou and A. Vasile, "Plutonium multirecycling in standard PWRs loaded with evolutionary fuels," *Nuclear Science and Engineering*, vol. 151, no. 1, p. 25, 2005.

[15] Foster *et al.*, "Review of PNL study on transmutation processing of high level waste," tech. rep., Los Alamos National Laboratory, 1974. LA-UR 74-74.

[16] M. Salvatores, I. Slessarev, G. Ritter, P. Fougeras, A. Tchistiakov, G. Youinou, and A. Zaetta, "Long-lived radioactive waste transmutation and the role of accelerator driven (hybrid) systems," *Nuclear Instruments and Methods in Physics Research Section A: Accelerators, Spectrometers, Detectors and Associated Equipment*, vol. 414, no. 1, pp. 5 – 20, 1998.

[17] G. S. Bauer, "Physics and technology of spallation neutron sources," *Nuclear Instruments and Methods in Physics Research Section A: Accelerators, Spectrometers, Detectors and Associated Equipment*, vol. 463, no. 3, pp. 505 – 543, 2001.

[18] NEA, "Accelerator-driven Systems (ADS) and Fast Reactors (FR) in Advanced Nuclear Fuel Cycles," tech. rep., OECD, 2002.

[19] M. Salvatores, "Nuclear fuel cycle strategies including partitioning and transmutation," *Nuclear Engineering and Design*, vol. 235, no. 7, pp. 805–816, 2005.

[20] Nuclear Energy Agency NEA, "Actinide and fission product partitioning and transmutation," tech. rep., OECD, 2003. EUR 20618 EN.

[21] GEN-IV, "Charter of the Generation IV International Forum," Retrieved in February 2012. http://www.gen-4.org/PDFs/GIFcharter.pdf.

[22] US DOE Nuclear Energy Advisory Committee and the Generation IV International Forum, "A Technology Roadmap for Generation IV Nuclear Energy Systems," tech. rep., GIF and DOE, 2002. GIF-002-00.

[23] J. Wallenius, E. Suvdantsetseg, and A. Fokau, "ELECTRA: European Lead-Cooled Training Reactor," *Nuclear Technology*, vol. 177, pp. 303–313, 2012.

[24] J. Kittel, B. Frost, J. Mustelier, K. Bagley, G. Crittenden, and J. Van Dievoet, "History of fast reactor fuel development," *Journal of Nuclear Materials*, vol. 204, pp. 1–13, 1993.

[25] T. Chikalla, C. McNeilly, and R. Skavdahl, "The plutonium-oxygen system," *Journal of Nuclear Materials*, vol. 12, no. 2, pp. 131–141, 1964.

[26] M. Kato, K. Morimoto, H. Sugata, K. Konashi, M. Kashimura, and T. Abe, "Solidus and liquidus temperatures in the UO_2-PuO_2 system," *Journal of Nuclear Materials*, vol. 373, no. 1-3, pp. 237–245, 2008.

[27] F. De Bruycker, K. Boboridis, P. Poml, R. Eloirdi, R. Konings, and D. Manara, "The melting behaviour of plutonium dioxide: A laser-heating study," *Journal of Nuclear Materials*, 2011.

[28] C. Ronchi, M. Sheindlin, M. Musella, and G. Hyland, "Thermal conductivity of uranium dioxide up to 2900 K from simultaneous, measurement of the heat capacity and thermal diffusivity," *Journal of Applied Physics*, vol. 85, p. 776, 1999.

[29] C. Duriez, J. Alessandri, T. Gervais, and Y. Philipponneau, "Thermal conductivity of hypostoichiometric low Pu content (U,Pu)O_{2-x} mixed oxide," *Journal of Nuclear Materials*, vol. 277, no. 2-3, pp. 143–158, 2000.

[30] J. Carbajo, G. Yoder, S. Popov, and V. Ivanov, "A review of the thermophysical properties of MOX and UO_2 fuels," *Journal of Nuclear Materials*, vol. 299, no. 3, pp. 181–198, 2001.

[31] C. Till and Y. Chang, "Evolution of the liquid metal reactor: the Integral Fast Reactor (IFR) concept," tech. rep., Argonne National Laboratory, USA, 1989. CONF-890425-3.

[32] C. McPheeters, R. Pierce, and T. Mulcahey, "Application of the pyrochemical process to recycle of actinides from LWR spent fuel," *Progress in Nuclear Energy*, vol. 31, no. 1, pp. 175–186, 1997.

[33] Y. S. Touloukian, P. E. Liley, and S. C. Saxena, *Thermophysical Properties of Matter*, vol. 1. IFI/Plenum, 1970.

[34] R. De Coninck, W. Van Lierde, and A. Gijs, "Uranium carbide: Thermal diffusivity, thermal conductivity and spectral emissivity at high temperatures," *Journal of Nuclear Materials*, vol. 57, no. 1, pp. 69–76, 1975.

[35] J. Wallenius private communication, 2012.

[36] S. Ross, M. El-Genk, and R. Matthews, "Uranium nitride fuel swelling correlation," *Journal of Nuclear Materials*, vol. 170, no. 2, pp. 169–177, 1990.

[37] S. Hayes, J. Thomas, and K. Peddicord, "Material property correlations for uranium mononitride: III. Transport properties," *Journal of Nuclear Materials*, vol. 171, no. 2-3, pp. 289–299, 1990.

[38] Y. Arai, Y. Suzuki, T. Iwai, and T. Ohmichi, "Dependence of the thermal conductivity of (U, Pu)N on porosity and plutonium content," *Journal of Nuclear Materials*, vol. 195, no. 1-2, pp. 37–43, 1992.

[39] T. Nishi, M. Takano, A. Itoh, M. Akabori, K. Minato, and M. Kizaki, "Thermal diffusivity of Americium mononitride from 373 to 1473 K," *Journal of Nuclear Materials*, vol. 355, no. 1, pp. 114–118, 2006.

[40] A. Santamarina, D. Bernard, P. Blaise, M. Coste, A. Courcelle, T. Huynh, C. Jouanne, P. Leconte, O. Litaize, S. Mengelle, *et al.*, "The JEFF-3.1.1 Nuclear Data Library," tech. rep., OECD NEA Report, 6807, 2009.

[41] A. Koning, R. Forrest, M. Kellett, R. Mills, H. Henriksson, and Y. Rugama, "The JEFF-3.1 nuclear data library," *JEFF Report*, vol. 21, 2006.

[42] P. F. Rose, "ENDF-201: ENDF/B-VI summary documentation," tech. rep., Brookhaven National Laboratory, Upton, NY, USA), 1991.

[43] R. K. Meulekamp and S. C. van der Marck, "Calculating the effective delayed neutron fraction with Monte Carlo," *Nuclear Science and Engineering*, vol. 152, no. 2, pp. 142–148, 2006.

[44] D. B. Pelowitz, "MCNPX User's Manual, Version 2.6.0," tech. rep., LA-CP-07-1473 (April 2008).

[45] J. F. Breismeister *et al.*, "MCNP-A General Monte Carlo N-Particle Transport Code, Version 4A," *LA-12625, Los Alamos National Laboratory*, 1997.

[46] T. E. Booth, H. G. Hughes, A. Zukaitis, F. B. Brown, R. D. Mosteller, M. Boggs, J. S. Bull, R. E. Prael, R. Martz, R. A. Forster, A. Sood, J. T. Goorley, and J. E. Sweezy, "MCNP - A General Monte Carlo N-Particle Transport Code, Version 5," tech. rep., LA-UR-03-1987 (April 2003).

[47] D. B. Pelowitz, J. S. Hendricks, J. W. Durkee, M. L. Fensin, M. R. James, G. W. McKinney, S. G. Mashnik, and L. S. Waters, "MCNPX 2.7. A Extensions," tech. rep., Los Alamos National Laboratory Report, LA-UR-08-07182, 2008.

[48] J. Leppänen, *Development of a New Monte Carlo Reactor Physics code*. PhD thesis, Helsinki University of Technology, 2007. VTT Publication 640.

[49] E. Woodcock, T. Murphy, P. Hemmings, and S. Longworth, "Techniques used in the GEM code for Monte Carlo neutronics calculations in reactors and other systems of complex geometry," in *Proceedings from Conference on Applications of Computing Methods to Reactor Problems*, p. 557, 1965.

[50] J. Leppänen, "Performance of Woodcock delta-tracking in lattice physics applications using the Serpent Monte Carlo reactor physics burnup calculation code," *Annals of Nuclear Energy*, vol. 37, no. 5, pp. 715 – 722, 2010.

[51] J. Leppänen, "PSG2 / Serpent - a continuous-energy Monte Carlo reactor physics burnup calculation code," tech. rep., VTT Technical Research Center of Finland, 2012.

[52] J. Leppänen private communication, 2012.

[53] J. E. Cahalan, "SAS4A/SASSYS-1 Maintenance and operation handbook," tech. rep., Argon National Laboratory, 2001.

[54] J. Klug *et al.*, "SCANDAL – a facility for elastic neutron scattering studies in the 50-130 MeV range," *Nuclear Instruments and Methods in Physics Research Section A*, vol. 489, no. 1-3, pp. 282 – 303, 2002.

[55] J. Klug, J. Blomgren, A. Ataç, B. Bergenwall, A. Hildebrand, C. Johansson, P. Mermod, L. Nilsson, S. Pomp, U. Tippawan, K. Elmgren, N. Olsson, O. Jonsson, A. V. Prokofiev, P.-U. Renberg, P. Nadel-Turonski, S. Dangtip, P. Phansuke, M. Österlund, C. Le Brun, J. F. Lecolley, F. R. Lecolley, M. Louvel, N. Marie-Noury, C. Schweitzer, P. Eudes, and F. Haddad, "Elastic neutron scattering at 96 MeV from C12 and Pb208," *Physical Review C*, vol. 68, p. 064605, Dec 2003.

[56] C. Johansson, J. Blomgren, A. Ataç, B. Bergenwall, S. Dangtip, K. Elmgren, A. Hildebrand, O. Jonsson, J. Klug, P. Mermod, P. Nadel-Turonski, L. Nilsson, N. Olsson, S. Pomp, A. V. Prokofiev, P.-U. Renberg, U. Tippawan, and M. Österlund, "Forward-angle neutron-proton scattering at 96 MeV," *Physical Review C*, vol. 71, p. 024002, Feb 2005.

[57] P. Mermod, J. Blomgren, C. Johansson, A. Öhrn, M. Österlund, S. Pomp, B. Bergenwall, J. Klug, L. Nilsson, N. Olsson, *et al.*, "95 MeV neutron scattering on hydrogen, deuterium, carbon, and oxygen," *Physical Review C (2006)*, vol. 74, p. 054002, 95.

[58] A. Öhrn, J. Blomgren, P. Andersson, A. Ataç, C. Gustavsson, J. Klug, P. Mermod, S. Pomp, P. Wolniewicz, M. Österlund, L. Nilsson, B. Bergenwall, K. Elmgren, N. Olsson, U. Tippawan, S. Dangtip, P. Phansuke, P. Nadel-Turonski, O. Jonsson, A. Prokofiev, P.-U. Renberg, V. Blideanu, C. L. Brun, J. F. Lecolley, F. R. Lecolley, M. Louvel, and N. Marie-Noury, "Elastic scattering of 96 MeV neutrons from iron, yttrium, and lead," *Physical Review C*, vol. 77, p. 024605, Feb 2008.

[59] P. Andersson, M. Tesinsky, C. Gustavsson, J. Blomgren, S. Pomp, R. Bevilaqua, A. Kolozhvari, F. R. Lecolley, N. Marie, Y. Naitou, M. Österlund, A. Prokofiev, V. Simutkin, U. Tippawan, and Y. Watanabe, "An upgrade of the SCANDAL facility for neutron scattering measurements at 175 MeV," *In manuscript*.

[60] D. Toprek, D. Reistad, B. Lundstrom, and D. Wessman, "Design of the central region in the Gustaf Werner cyclotron at the Uppsala University," *Nuclear Instruments and Methods in Physics Research Section A*, vol. 486, no. 3, pp. 539 – 544, 2002.

[61] A. V. Prokofiev, J. Blomgren, O. Bystrom, C. Ekstrom, S. Pomp, U. Tippawan, V. Ziemann, and M. Österlund, "The TSL neutron beam facility," *Radiation Protection Dosimetry*, vol. 126, no. 1 - 4, pp. 18 – 22, 2007.

[62] A. Prokofiev, M. Chadwick, S. Mashnik, N. Olsson, and L. Waters, "Development and validation of the $^{7}Li(n,p)$ nuclear data library and its application in monitoring of intermediate energy neutrons," *Nuclear Science and Technology*, vol. Supplement 2, pp. 112 – 115, 2002.

[63] S. Dangtip *et al.*, "A facility for measurements of nuclear cross sections for fast neutron cancer therapy," *Nuclear Instruments and Methods in Physics Research Section A*, vol. 452, no. 3, pp. 484 – 504, 2000.

[64] A. Alemberti, J. Carlsson, E. Malambu, A. Orden, L. Cinotti, D. Struwe, P. Agostini, and S. Monti, "ELSY – European LFR Activities," *Journal of Nuclear Science and Technology*, vol. 48, no. 4, pp. 479–482, 2011.

[65] A. Alemberti, J. Carlsson, E. Malambu, A. Orden, D. Struwe, P. Agostini, and S. Monti, "European lead fast reactor – ELSY," *Nuclear Engineering and Design*, 2011.